Theses and Dissertations                      1. Thesis and Dissertation Collection, all items

2004-12

# Improvement of an acoustic sounder device used to measure atmospheric turbulence

## Liu, Jeng-Shiung

Monterey, California. Naval Postgraduate School

http://hdl.handle.net/10945/1221

# NAVAL POSTGRADUATE SCHOOL

## MONTEREY, CALIFORNIA

# THESIS

**IMPROVEMENT OF AN ACOUSTIC SOUNDER DEVICE USED TO MEASURE ATMOSPHERIC TURBULENCE**

by

Jeng-Shiung Liu

December 2004

| | |
|---|---|
| Thesis Advisor: | Thomas J. Hofler |
| Co-Advisor: | Donald L. Walters |

**Approved for public release; distribution is unlimited**

THIS PAGE INTENTIONALLY LEFT BLANK

| REPORT DOCUMENTATION PAGE | | *Form Approved OMB No. 0704-0188* |
|---|---|---|

Public reporting burden for this collection of information is estimated to average 1 hour per response, including the time for reviewing instruction, searching existing data sources, gathering and maintaining the data needed, and completing and reviewing the collection of information. Send comments regarding this burden estimate or any other aspect of this collection of information, including suggestions for reducing this burden, to Washington headquarters Services, Directorate for Information Operations and Reports, 1215 Jefferson Davis Highway, Suite 1204, Arlington, VA 22202-4302, and to the Office of Management and Budget, Paperwork Reduction Project (0704-0188) Washington DC 20503.

| 1. AGENCY USE ONLY (*Leave blank*) | 2. REPORT DATE<br>December 2004 | 3. REPORT TYPE AND DATES COVERED<br>Master's Thesis | |
|---|---|---|---|
| **4. TITLE AND SUBTITLE**: Improvement of an Acoustic Sounder Device Used to Measure Atmospheric Turbulence | | **5. FUNDING NUMBERS** | |
| **6. AUTHOR(S)** Liu, Jeng-Shiung | | | |
| **7. PERFORMING ORGANIZATION NAME(S) AND ADDRESS(ES)**<br>Naval Postgraduate School<br>Monterey, CA 93943-5000 | | **8. PERFORMING ORGANIZATION REPORT NUMBER** | |
| **9. SPONSORING /MONITORING AGENCY NAME(S) AND ADDRESS(ES)**<br>N/A | | **10. SPONSORING/MONITORING AGENCY REPORT NUMBER** | |

**11. SUPPLEMENTARY NOTES** The views expressed in this thesis are those of the author and do not reflect the official policy or position of the Department of Defense or the U.S. Government.

| 12a. DISTRIBUTION / AVAILABILITY STATEMENT<br>Approved for public release; distribution is unlimited. | 12b. DISTRIBUTION CODE |
|---|---|

**13. ABSTRACT (maximum 200 words)**

Optical turbulence plays an important role in the propagation of electromagnetic waves through the atmosphere because it broadens and distorts the optical beam. A variety of optical, thermal, and acoustic instruments are used to detect the atmospheric turbulence and an acoustic echosounder has proven to be a valuable tool to probe the fine dynamic structure of atmospheric turbulence within first hundred meters above the surface.

The first planar acoustic echosounder constructed at the Naval Postgraduate School was by Weingartner and Wroblewski, under Walters' supervision. Moxcey later modified this design by reducing the number of drivers from 25 to 19 and placing the drivers closer together into a hexagonal, close-packed array. This thesis explored the potential sources of the transducer ringing and implemented solutions to the problem. Additionally, we also improved the receiving sensitivity of the echosounder and lowered the electronics noise when receiving. Finally, we applied these techniques to another array assembled with new drivers to improve its performance compared to the previous echosounder array, while measuring and quantifying the level of improvement achieved.

| 14. SUBJECT TERMS<br>Acoustic echosounder, Acoustic sounder, transducer | | | 15. NUMBER OF PAGES<br>71 |
|---|---|---|---|
| | | | 16. PRICE CODE |
| 17. SECURITY CLASSIFICATION OF REPORT<br>Unclassified | 18. SECURITY CLASSIFICATION OF THIS PAGE<br>Unclassified | 19. SECURITY CLASSIFICATION OF ABSTRACT<br>Unclassified | 20. LIMITATION OF ABSTRACT<br>UL |

THIS PAGE INTENTIONALLY LEFT BLANK

# IMPROVEMENT OF AN ACOUSTIC SOUNDER DEVICE USED TO MEASURE ATMOSPHERIC TURBULENCE

Jeng-Shiung Liu
Lieutenant Commander, Republic of China Navy
B.S., Chinese Naval Academy, 1992

Submitted in partial fulfillment of the
requirements for the degree of

## MASTER OF SCIENCE IN APPLIED PHYSICS

from the

## NAVAL POSTGRADUATE SCHOOL
**December 2004**

Author:               Jeng-Shiung Liu

Approved by:       Thomas J. Hofler
Thesis Advisor

Donald L. Walters
Co-Advisor

James H. Luscombe
Chairman, Department of Physics

THIS PAGE INTENTIONALLY LEFT BLANK

# ABSTRACT

Optical turbulence plays an important role in the propagation of electromagnetic waves through the atmosphere because it broadens and distorts the optical beam. A variety of optical, thermal, and acoustic instruments are used to detect the atmospheric turbulence and an acoustic echosounder has proven to be a valuable tool to probe the fine dynamic structure of atmospheric turbulence within first hundred meters above the surface.

The first planar acoustic echosounder constructed at the Naval Postgraduate School was by Weingartner and Wroblewski, under Walters' supervision. Moxcey later modified this design by reducing the number of drivers from 25 to 19 and placing the drivers closer together into a hexagonal, close-packed array. Although the acoustic echosounder works well, there are problems with resonances and ringing in the current choice of transducers. This thesis explored the potential sources of the transducer ringing and implemented solutions to the problem. Additionally, we also improved the receiving sensitivity of the echosounder and lowered the electronics noise when receiving. Finally, we applied these techniques to another array assembled with new drivers to improve its performance compared to the previous echosounder array, while measuring and quantifying the level of improvement achieved.

THIS PAGE INTENTIONALLY LEFT BLANK

# TABLE OF CONTENTS

THIS PAGE INTENTIONALLY LEFT BLANK

# LIST OF FIGURES

THIS PAGE INTENTIONALLY LEFT BLANK

# LIST OF TABLES

THIS PAGE INTENTIONALLY LEFT BLANK

# ACKNOWLEDGMENTS

I would like to express my deepest gratitude and sincere appreciation to those who, through their guidance and assistance, made this work possible. First I would like to thank Professor Walters, my thesis co-advisor who provided opportunity, support and advice. Additionally, I would like to thank Professor Hofler, my thesis advisor. Without his overwhelming assistance, advice and guidance throughout the process of this thesis, I doubt I ever would have been able to accomplish this task.

Above all, I would like to express my heartfelt thanks to my loving and devoted wife, Hsiang-Yi. Her patience, understanding, and remarkable ability to maintain a pleasant, comforting home during this highly stressful time made this process possible.

THIS PAGE INTENTIONALLY LEFT BLANK

# I.     INTRODUCTION

## A.     THE OPTICAL PROPAGATION PROBLEM

Optical turbulence plays an important role in the propagation of electromagnetic waves through the atmosphere because it introduces random phase distortions that increase the divergence of the energy. Optical turbulence is the result of fluctuations in the index of refraction induced by atmospheric velocity perturbations (Ref. 1). The index of refraction of the atmosphere depends on the atmospheric temperature, humidity, pressure and wind shear. Therefore, it may vary from point to point in space because of the fluctuation of any of the parameters. When electromagnetic waves propagate through the turbulent region, the turbulence-induced fluctuations distort the phase of the wave.

Turbulent phenomena exist at all levels of the atmosphere. Near the surface, a considerable portion of the optical turbulence along a vertical path results from the heat flux interchange between the earth's surface and the air. During the day the heating of the surface results in non-uniform convection and yields vertical thermal plumes. These thermal plumes rise continuously in the atmosphere, gradually mixing and increasing the temperature of the lower atmosphere. Hence, strong optical turbulence occurs. At night the process reverses. The surface cools by radiation, is cooler than the air and wind shear creates optical turbulence. This cooling process is generally less turbulent than the heating process (Ref. 2).

## B.     MEASUREMENT OF ATMOSPHERIC TURBULENCE

### 1.     Refractive Index Structure Parameter

Turbulence effects are subject to variations in the atmospheric parameters, such as the wind speed, temperature, and the index of refraction. One of the critical parameters for describing optical turbulence is the refractive index structure parameter, $C_n^2$, which is the value of the mean squared statistical average of the difference between the indices of refraction at two different points divided by the point's separation (Ref. 3). The refractive index structure parameter has the form:

$$C_n^2 = \frac{\left\langle (n_2 - n_1)^2 \right\rangle}{r^{2/3}} \quad , \tag{1}$$

where $n_1$ and $n_2$ are the indices of refraction at points 1 and 2 respectively, and $r$ is the separation between points 1 and 2 in the atmosphere.

However, $C_n^2$ itself is very difficult to measure directly and an easier way is to measure the temperature structure parameter, $C_T^2$. Tatarski (Ref. 4) derived a useful relationship between $C_n^2$ and $C_T^2$ :

$$C_n^2 = \left( \frac{79 \times 10^{-6} P}{T^2} \right)^2 C_T^2 \quad , \tag{2}$$

where P is the atmospheric pressure in mbar and T is the temperature in Kelvin.

The reference standard for measuring optical turbulence is to use microthermal probe sensors. This direct measure of $C_T^2$ uses the difference in temperature between two fine wires that are a few microns in diameter, 5-10 mm long and are separated by 50 to 100 cm. Although straightforward to implement, the fragility of the wires makes microthermal probes unsuitable for atmospheric characterization. Rain and airborne debris quickly break the wires, and contamination of the fine wires by dust and airborne contaminants increase the thermal time constant (Ref. 5).

## 2. Optical Instrument Measurement

A variety of optical, thermal, and acoustic instruments are used to detect the atmospheric turbulence. Optical systems developed by Walters (Refs. 6 and 7), Professor at the Naval Postgraduate School, can measure accurately two optical parameters, the spatial length ($r_0$) and the isoplanatic angle ($\theta_0$), which are measures of the fluctuations of electromagnetic waves through the atmosphere. However, the data collected by this optical system lacks the altitude dependence, and optical instruments are often more complicated and expensive to operate. The lack of resolution along the optical path is a serious limitation since local sources of turbulence are masked by the path-averaged measurements.

### 3. Acoustic Echosounder Measurement

An acoustic echosounder has proven to be a valuable tool to probe the atmospheric turbulence within the first hundred meters above the surface. It transmits a pulse of acoustic energy into the atmosphere and uses acoustic waves scattered by atmospheric density and velocity fluctuations resulting from wind shears, humidity variations and temperature inversions to measure changes in the index of refraction of the atmosphere. The power returned from these turbulent structures, $P_R$, is proportional to the power transmitted, $P_T$. The equation relating these terms has been summarized by Neff (Ref. 8) as below

$$\frac{P_R}{E_R} = [P_T E_T]\left[e^{-2\alpha R}\right]\sigma_0(R,f)\left[\frac{c\tau}{2}\right]\left[\frac{A}{R^2}G\right] \quad , \tag{3}$$

where

- $\dfrac{P_R}{E_R}$ is the received acoustic power ($P_R$ is the measured electrical power from a range R and $E_R$ is the efficiency of conversion from received acoustic power to electrical power),

- $P_T E_T$ is the transmitted acoustic power ($P_T$ is the electrical power applied to the transducer at frequency f and $E_T$ is the efficiency of conversion from electrical driving power to radiated acoustic power),

- $e^{-2\alpha R}$ is the round trip power loss resulting from attenuation by air where $\alpha$ is the average attenuation $(m^{-1})$ to the scattering volume at range R (m),

- $\sigma_0$ (R,f) is the acoustic backscattering cross section per unit volume at a distance R (m) and frequency f. $(s^{-1})$,

- $c\tau/2$ is the maximum effective scattering volume thickness where c is the local speed of sound $(ms^{-1})$ and $\tau$ is the acoustic pulse length (s),

- $AG/R^2$ is the solid angle subtended by the antenna aperture A $(m^2)$ at range R (m) from the scattering volume, modified by an effective aperture factor G, resulting from the antenna's directivity and geometry.

Tatarski derived the acoustic backscattering cross section per unit volume, $\sigma_0$ (R, f) at 180°

$$\sigma_0(R,f) = 0.0039 k^{1/3} \left( \frac{C_T^2}{T^2} \right) \quad , \tag{4}$$

where

k is the acoustic wavenumber (m$^{-1}$),

T is the local mean temperature (K),

$C_T^2$ is the temperature structure parameter.

The acoustic backscattering cross section is proportional to the acoustic wavenumber and the temperature structure parameter. Combing Equations (3) and (4), and solving for $C_T^2$ yields

$$C_T^2 = \left[ \frac{1}{0.0039} \right] \left[ \frac{1}{E_R E_T} \right] \left[ \frac{T^2}{k^{1/3}} \right] \left[ \frac{P_R}{P_T} \right] \left[ \frac{2}{c\tau} \right] \left[ \frac{1}{AG} \right] R^2 e^{-2\alpha R} \quad . \tag{5}$$

When $C_T^2$ is obtained, then the refractive index structure parameter $C_n^2$ is available via Equation (2).

The attenuation exponent $\alpha$ is typically a strong function of frequency and humidity, with the higher frequencies being attenuated more than lower frequencies. Extremely low humidity in the 10-20% range exhibit very high absorption compared to moist environments (Ref. 9).

### 4.    Acoustic Detection Limitations

Our interest is the strong optical turbulence located near the earth's surface. An acoustic echosounder operating between 2000 and 5000 Hz is suitable for probing the turbulent structures with the first few hundred meters above the ground. Atmospheric turbulence produces Bragg scattering of the acoustic energy, so the dominant scale that contributes to scattering is the acoustic wavelength divided by 2. This corresponds to 4 cm for a 4000 Hz acoustic wave.

Because the echo sounder transducers are mechanical devices with inertia and restoring forces, they continue to ring after the electrical pulse stops. Since the same transducer is used to produce the acoustic wave and to detect the scattered energy, a significant recovery time occurs as while the mechanical ringing decays. The actual minimum detection range is typically a factor of 30-60 times farther than the electrical pulse length.

Whether a given object will be detected depends upon the strength of the returned signal relative to the strength of the background noise and interference signals, that is, the signal-to-noise ratio. A poor signal-to-noise ratio reduces the maximum detection range. Therefore, the greater the improvement in signal-to-noise ratio, the greater the detection range.

The magnitude of the exponential attenuation coefficient $\alpha$ controls the maximum detection range. This coefficient increases at higher frequencies so lowering the operating frequency will increase the range. This has the disadvantage of increasing the size of the array to maintain a similar acoustic beam divergence. In addition, the minimum range usually increases because the transmitted pulse exponential recovery time increases at lower frequencies.

## C.    PREVIOUS WORK

### 1.    General

The first planar acoustic echosounder constructed at the Naval Postgraduate School was by Weingartner (Ref. 10) and Wroblewski (Ref. 11), under Walters' supervision. It was a 25 driver, square, planar array enclosed within a rectangular acoustically absorbent shroud and was an effective tool for probing the lower atmosphere. Moxcey later modified this design by reducing the number of drivers from 25 to 19 and placing the drivers closer together into a hexagonal, close-packed array. Furthermore, in order to reduce the side lobes, a Rubbermaid brand 55 gallon plastic trash container with lead lined semi porous foam attached along the inside surface was chosen as an additional outer enclosure. The appearance of an acoustic echosounder is illustrated in Figure 1. The experimental results demonstrated that the hexagonal packed planar

acoustic echosounder significantly reduced the side lobes and concentrated energy into the main lobe.



Figure 1.        A photograph of an acoustic echosounder (from Walters).

## 2.        Problem Description

The above measures improved the performance of the acoustic echosounder, but there were still some problems concerning the planar array to be solved. Firstly, the transducer ringing following the transmitted pulse limited the minimum detection range to 15 m.

Secondly, while electronic noise from the pre-amplifier circuit was relatively low, the maximum detection range was sometimes limited by it. In most instances, the dominant noise is environmental and its sources include: wind flow noise over the outer array enclosure and nearby trees or scrub brush; birds and aircraft; and nearby footsteps, voices, and autos.

The effect of environmental noise sources can only be minimized in two ways. Either transmits more acoustic energy in order to increase the desired reflected signal, and/or reduce the bandwidth of the array-preamplifier system to the minimum required by the signal processing of the desired signal. The minimum bandwidth is roughly 400 to 500 Hz and is determined largely by wind generated Doppler shift and Fourier broadening of the short transmitted pulse.

Over the last decade, different acoustic transducers have been used because of changes in the manufacture's design or the manufacture has changed because the source has moved off shore. The original Motorola piezo transducer source (US) became CTS (Mexico) in the mid 1990's and now the only source is Mainland China. Each change has introduced a unique set of compromises that affected the design of the sonar system. Moving from the Motorola to the CTS manufactured units increased the recovery time of the array of sonar system from 20 ms to over 100 ms. This increased the minimum range from 4 m to 15 meters, but the reason of this change was not clear.


**D.    OBJECTIVES**

The main objective for the work in this thesis was to explore the potential causes of the transducer array ringing and find possible solutions to the long decay time. Additionally, we also tried to improve the receiving sensitivity by lowering the electronics noise of the echosounder. Finally, we fabricated another array assembled with new drivers to improve its performance compared to previous echosounder arrays, while measuring and quantifying the level of improvement achieved.

THIS PAGE INTENTIONALLY LEFT BLANK

# II.     THEORETICAL CONSIDERATIONS

## A.     EQUIVALENT CIRCUITS
### 1.     Basic PZT Transducer

The array consists of 19 CTS brand drivers and the transduction element of the driver is a bilaminar PZT (Lead Zirconate Titanate) flexural disk; thus we can treat it as a piezoelectric-type transducer. For maximum transmit efficiency the driver is usually operated near its fundamental resonant frequency. By impedance analogy with electrical components, an equivalent circuit around resonance that is used to represent a simple piezoelectric transducer is shown in Figure 2. The circuit shows the connection between the mechanical behavior of the transducer and its electrical characteristics.
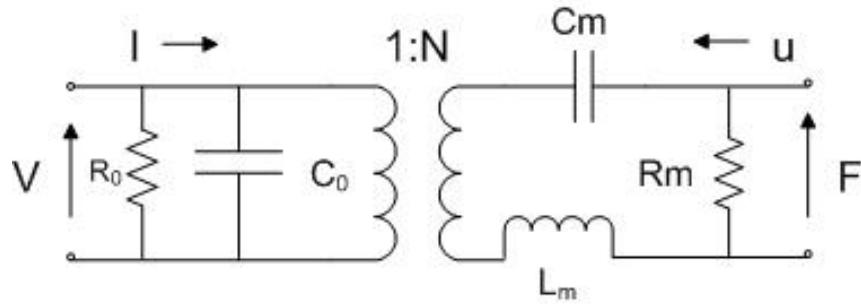


$R_0$ = blocked resistance          $R_m$ = motional resistance

$C_0$ = blocked capacitance     $C_m$ = motional capacitance

$L_m$ = motional inductance

Figure 2.          An equivalent circuit for a simple piezoelectric transducer (After: Ref. 12).

When a transducer is operated around mechanical resonance, the blocked leakage conductance $1/R_0$ is very small ($R_0$ is very large) compared to the susceptance term $\omega C_0$; therefore, it can be ignored for simplifying the equivalent circuit. A further simplified equivalent circuit can be shown in Figure 3. The electrical input admittance of the circuit is given by (Ref. 12)

9
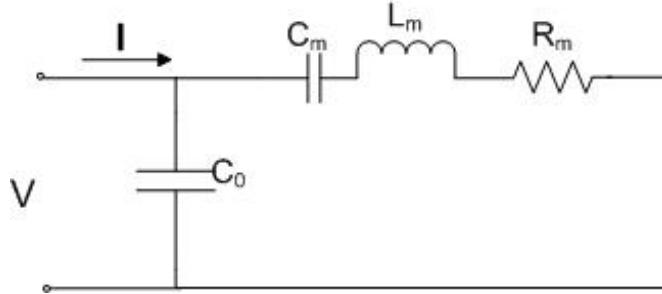
Figure 3.    A simplified equivalent circuit for a simple piezoelectric transducer
around resonance (From: Ref. 12).

$$Y_{in} = j\omega C_0 + \cfrac{1}{R_m + j\left(\omega L_m - \cfrac{1}{\omega C_m}\right)} \qquad . \qquad (6)$$

At mechanical resonance the reactance of the motional impedance vanishes and
the circuit appears as $C_o$ in parallel with $R_m$. Thus the input admittance at mechanical
resonance becomes

$$Y_{in} = j\omega C_0 + \frac{1}{R_m} \qquad . \qquad (7)$$

The average power delivered to a transducer is proportional to the conductance
term $1/R_m$. Theoretically, to transfer the maximum power we can add an inductor in
parallel with the capacitor $C_0$, so the reactance of the load at resonance vanishes and
appears purely resistive.

### 2.    Inductive Tuning

The diameter of the paper cone attached to the bilaminar PZT disk is 3.34 cm,
which is smaller than the acoustic wavelength at our operating frequency (4100 Hz);
hence the incident acoustic pressure is uniformly distributed over the active part of the
disk. Under this condition, the receiving sensitivity of our array is simply the ratio of the
output from the electrical terminals to the acoustic pressure.

An equivalent circuit for a tuned piezoelectric transducer used as a receiver is
shown in Figure 4.

10
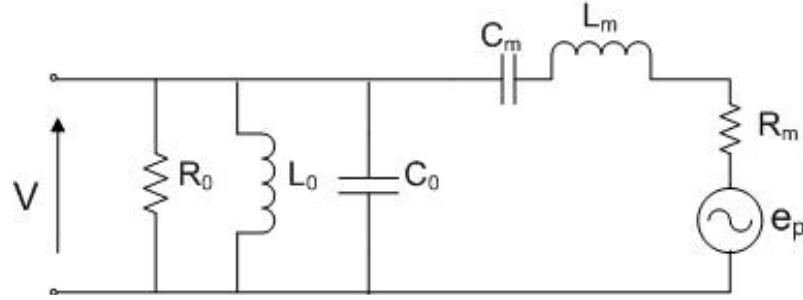
Figure 4. An equivalent circuit for a tuned piezoelectric transducer used as a receiver. Note that $L_0$ is an added tuning inductor (From: Ref. 13).

To understand the effect of adding a parallel tuning inductor, we use the standard version "SPICE" software (Ref. 14) to do computer analysis. The following circuit (Figure 5) is a reasonable equivalent circuit for a PZT bilaminar flex disk transducer with horn based on parameter measured with an HP4194 impedance analyzer and a CTS tweeter. In the schematic, the tuning inductor L2 is set at 100 H, which means it's Z is negligible at high frequency. Components C1, R1, and L1 are the motional elements and C2 is the blocked capacitance. The transfer function (frequency response) from the signal source to the top of the tuning inductor is shown above right. The peak value is about -1.1 dB and the Q is about 5.25.
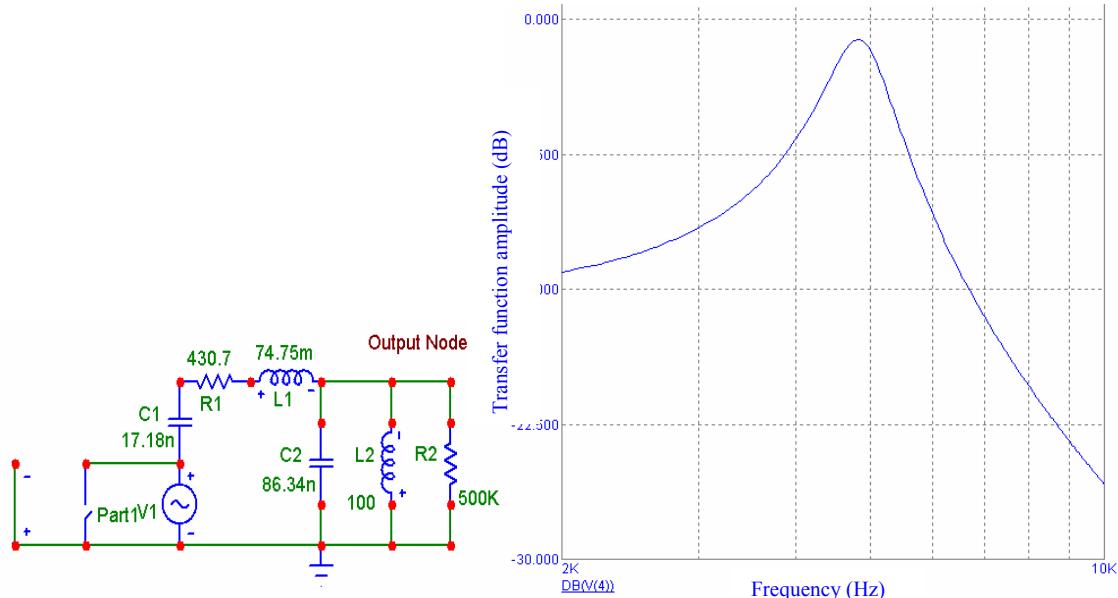


Figure 5. An equivalent circuit for an isolated, un-tuned piezoelectric transducer (left) and its frequency response (right). Note that the effect of the tuning inductor $L_2$ is ignorable.

11
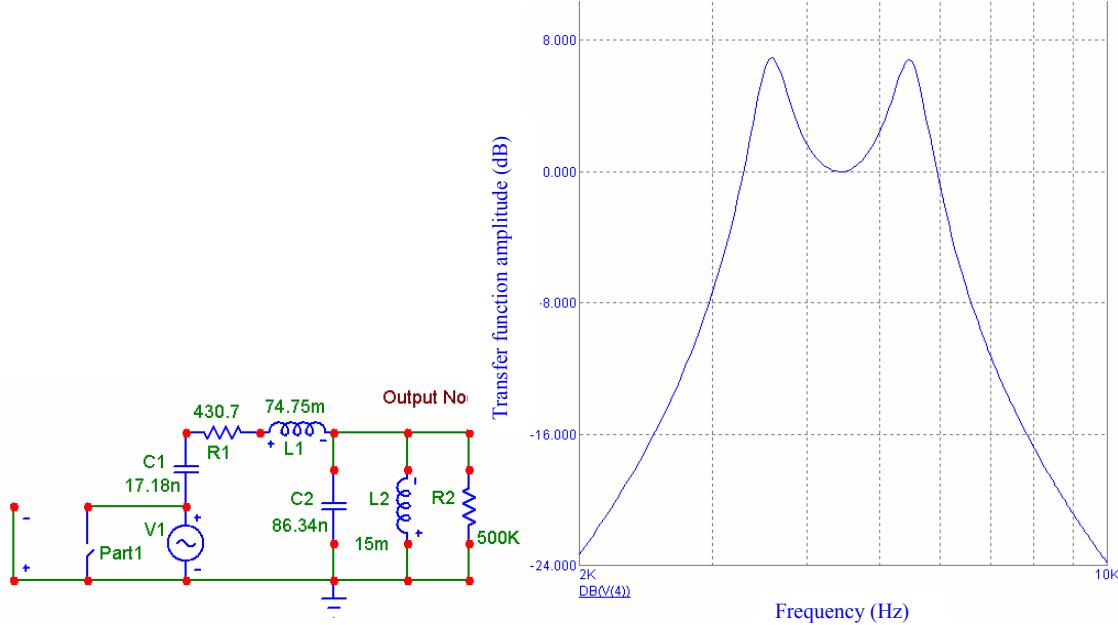
Figure 6. An equivalent circuit for a tuned piezoelectric transducer (left) and its frequency response (right). Note that the tuning inductor now is 15 mH.

Figure 6 shows a case where the inductance $L_2$= 15 mH provides optimal compensation for the reactive capacitance $C_2$. This splits the single resonance seen if Figure 5 into two resonances. The magnitude of the response is 3 to 10 db above the case without the inductor, Figure 5. Unfortunately, optimal tuning of $L_2$ introduces a new issue. The two resonance peaks provide the highest receive sensitivity around 3600 Hz and 5500 Hz that are different from the minimum at 4500 that provides the largest transmit response.

We note that that the single peak is split into two now, but also the response is generally between 0.0 and 7.0 dB, which is an increase of 3 to10 dB compared to Figure 5. This could be very valuable, although, since we now have a more complicated resonance structure.

It is also important to remember that increased sensitivity is basically useless if the un-tuned system had a receiving noise floor dominated by the mechanical resistance R1. If, on the other hand, the un-tuned noise floor is dominated by the preamplifier placed at the top of L2, then a boost in the sensitivity is possible.

12

From the above circuit analysis, we know that the tuning inductor not only increases the Receiving Voltage Sensitivity (RVS) but also results in a wider frequency response range. The bandwidth approximately increases from 1600 to 2300 Hz. In practical applications, we are interested in the bandwidth around the operating frequency and must avoid other frequencies outside this frequency range. Therefore, to have higher receiving sensitivity and narrower bandwidth, we must consider alternative circuits.

### 3. LC Load Tuning

#### a. *Environmental Noise*

Environmental noise discussed in the preceding chapter arises from undesirable external sounds that cover a broad spectrum. Because environmental noise is unavoidable, our concern with noise is not in trying to control the environmental noise received by the acoustic echosounder, but with limiting the frequency response range of the system to reduce the environmental noise contribution..

#### b. *Narrowing Bandwidth*

Figure 6 shows that adding a single inductor $L_2$ to suppress the reactive load of capacitor $C_2$, splits the mechanical resonance into two separated peaks. This has the disadvantage that the external noise sensitivity increases at the peak frequencies, which are different from the most efficient transmit frequency at the minima around 4500 Hz. One way to avoid this splitting is to increase the capacitance $C_2$ and use a smaller inductor for $L_2$. Figure 7 and 8 show the schematic and SPICE transfer function respectively. $C_2$ is the internal transducer shunting capacitance.
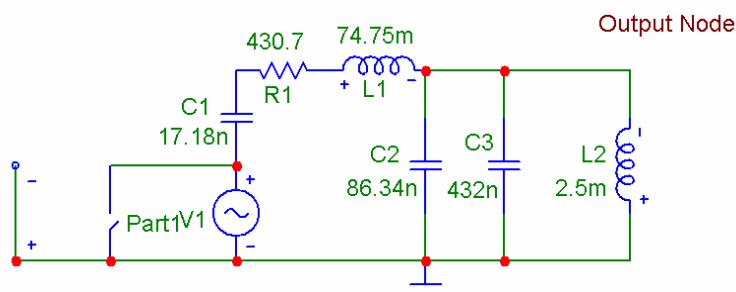


Figure 7.  An equivalent circuit for a tuned piezoelectric transducer with a combination of inductor L2 and capacitor C3.

13
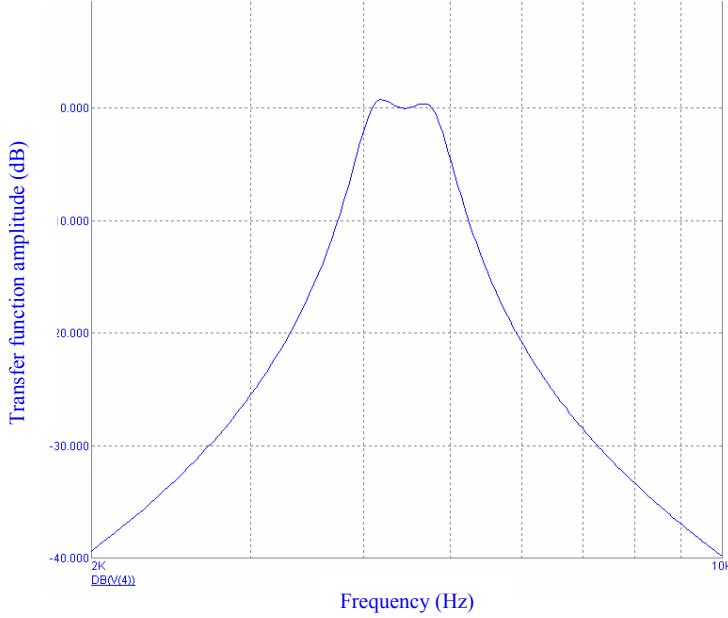
Figure 8.        Transfer function for a tuned piezoelectric transducer with a combination of smaller inductor and larger capacitor.

From the above plot, it can be seen that the two peaks seen in Figure 6 appear to approach each other. Responses are slightly bigger 0.0 dB, which is between that of a tuning inductor alone and that of no inductor. The bandwidth is about 1200 Hz, which is even smaller than that of no inductor. Thus, this LC combination not only increases the receiving sensitivity, but also avoids the broad noise bandwidth, while matching the electrical and mechanical resonance frequencies.

Finally, there may be a tradeoff between increasing RVS sensitivity and narrowing frequency response. The electrical currents flowing through the added parallel capacitor and inductor will be much higher in the narrow bandwidth configuration, and thus the dissipation caused by any non-ideal resistive behavior of the added electrical components may reduce the receiving sensitivity slightly. How to set the configuration of the LC loads will likely depend upon practical requirements.

## B.      WAVEFORM OF TRANSMITTED SIGNAL

The waveform of the transmitted signal influences the number of transducer resonant modes that are excited. A rectangular shaped sine wave burst has a sinc function spectrum centered on the sine wave frequency. The spectral breadth of the sinc function

14

can induce resonant modes well away from the operating frequency. Using a Gaussian or Hann waveform instead of the rectangular shape will reduce the spectral width of the transmitted pulse, reducing the number and magnitude of transducer resonant modes that are excited. This provides one way to decrease the array recovery time.

## C.    DIFFRACTION EFFECT

A sound is wave-like in nature, so there are many properties and characteristics of a light wave can also be found in a sound wave. According to Huygens' Principle, every point on the wavefront of a wave disturbance can be viewed a separate source of secondary spherical wavelets. During the propagation of sound waves, whenever the wavefront is unobstructed each element of the wavefront travels along a straight line, but when it suffers an obstacle or an aperture, the waves bend at the edge of obstacle or at aperture and the phenomena of diffraction occurs (Ref. 15).

The diffraction effect makes the narrow beam spread out, and the resulting angular width primarily depends upon the ratio of wavelength to dimension. The half-angle subtended by the main lobe can be estimated for rectangular geometry by (Ref. 16).

$$\sin\theta \cong \frac{\lambda}{L} = \frac{c}{Lf} \quad , \tag{8}$$

From the above expression it is quite clear that if we want to have a narrow beam, we either have a large-dimension transmitter or use a sufficiently high frequency.

Usually, the driver has high mechanical impedance. To match the impedance of the driver to that of the low impedance air and feed more power into the sound waves, a horn is used. Theoretically, the cross-sectional area of the horn is inversely proportional to the acoustic impedance. Thus the cross-sectional area of an ideal horn should increase so gradually that the wave travels forward without realizing changes in the guiding wall of the horn; otherwise, the wave will see fairly abrupt impedance changes and be reflected from the horn (Ref. 17).

In order to mount the drivers close together into an array, the outer edge of every horn was cut to form a hexagonal or circular shape.  The resulting edge was about 3 mm thick and made an angle of $90^O$ with respect to the flared horn.

15
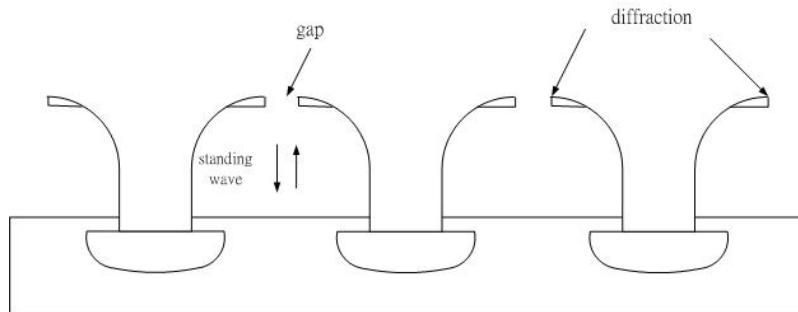
Figure 9.        The side view of array #2 for illustrating the effects of diffraction and standing waves.

When a sound wave produced by the piezo disk arrives at the outer edge of the horn, the sudden change in shape at the edge will scatter sound energy. In addition, a short distance away the edge of an adjacent horn will introduce new scattering sources (figure 9).

There are several significant effects due to diffraction that deserve attention. One is that when the diffracted waves from the edges combine with the original wave, interference occurs. It will give rise to amplitude variations of the sound pressure with respect to frequency and makes the distribution of the sound intensity with respect to radiation angle become irregular. The result of the effect is illustrated graphically in Figure 10.
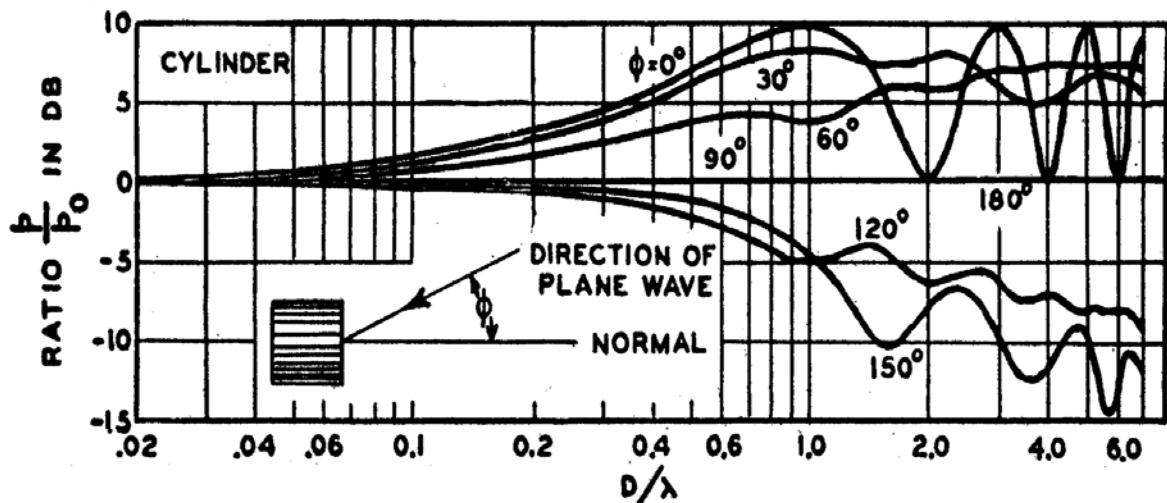


Figure 10.        The diffraction of a sound wave by a cylinder (From: Ref. 18).

16

The figure shows a calculation of the pressure response of a radiating point source placed on the center of a flat face of a solid right-cylinder. The pressure variation in the plot is a function of the ratio of the cylinder's diameter to the wavelength. With different incident angles, the interference of the reflected wave and the direct wave creates different received pressure amplitudes. It is apparent from the plot that when receiving on-axis and the value of the ratio is around 1, 3… and so on, the received pressure will be a maximum. For our driver, the diameter of the horn mouth is 7.6 cm and it suggests that the first maximum value occurs at a frequency of 4800 Hz for the ratio of unity. This means that there probably exists another peak in the RVS sensitivity at a frequency of 4800 Hz, in addition to the main RVS peak created by the PZT transducer. This result will be shown later in a measurement.

Another important phenomenon occurs when some fraction of the sound wave enters the interspaces between the back of the horn mouth and the top surface of the box, and standing waves are set up there. The relevant influences of standing waves will be discussed in the next section.

THIS PAGE INTENTIONALLY LEFT BLANK

# III.   EXPERIMENT AND DISCUSSION

## A.   EQUIPMENT DESCRIPTION

To perform a series of related data acquisition, measurements and analysis, several instruments were used, as follows:

- Stanford Research Systems SR785 two-channel dynamic signal analyzer used to measure FFT's of microphone and transducer signals, impedance and admittance of the individual driver and the array using a 1Volt/Ampere current transformer, as well as Transmitted Voltage Response (TVR) and Receiving Voltage Sensitivity (RVS),

- Hewlett Packard 33120A synthetic function generator used to generate the transmitted signal with square burst,

- Tektronics TDS 420 Digitizing Oscilloscope used to display and transfer the transmitted and received signals to a notebook computer via a GPIB interface,

- Dell Inspiron notebook also used to generate the transmitted signal with a Gaussian shaped tone burst,

- B&K 12 mm microphone and 12 mm condenser microphone, model 4136, used to receive transmitted signal,

- Transmitter-amplifier/Receiver-preamplifier circuit, which was adapted from Walters, and re-designed and constructed by Hofler, Professor at the Naval Postgraduate School, used to amplify transmitted and received signals. Figure 11 details the circuitry schematic.

Most of measurements were performed in the anechoic chamber in the basement (Spanagel Hall) at NPS. The surface of the walls, floor, and ceiling of this room is covered with fiberglass wedges that are highly absorbent, so the wave reflected from the boundary wall is negligibly small. Also, it insulates the chamber against all disturbing sounds from the outside.
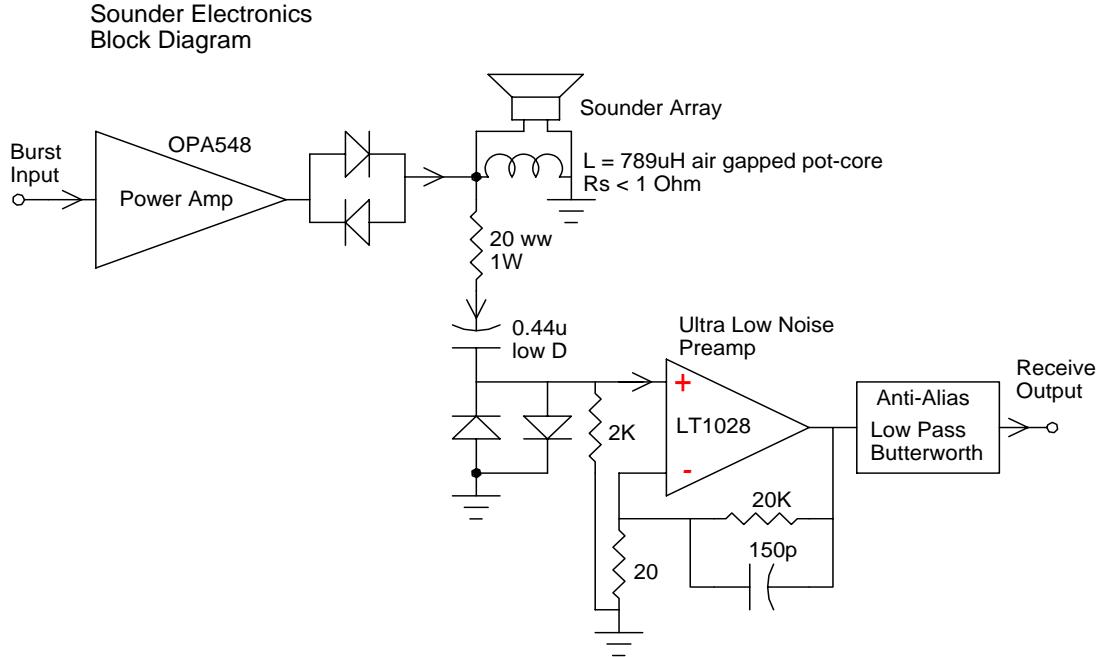
Figure 11.        Schematic of the transmitter-amplifier/receiver-preamplifier circuit (from Hofler).

## B.        TAP TESTING OF DRIVER HOUSING

When a voltage is applied to the driver, the bilaminar PZT disk and the attached cone vibrates and radiates sound waves into the horn and finally the open air. Transducer models fitted to measured data show that while the PZT disk and cone by itself had high quality factors, most of the dissipation in the modeled equivalent circuit of the whole driver comes from the enhanced radiation of the horn. From figure 5, we know that the resulting quality factor is roughly 5.3 for a single driver. According to the below expression (Ref. 16)

$$Q = \frac{1}{2}\omega_0\tau \quad , \tag{9}$$

We can calculate the resulting relaxation time τ of about 0.4 ms.

Based on this model, in 10 ms after a transmitted burst at 4200 Hz, the motion of the driver cone should be reduced by roughly 70 dB.  However, ring-down measurements show very considerable ringing after a 10 ms delay, which caused us to search for other sources of the ringing.

The driver cone is directly coupled to the acoustic volume velocity, the area times the velocity, projected into the throat of the driver horn, but it also couples to the volume velocity in the opposite direction. This backwards directed air motion is usually captured in a small rigidly housed "back volume" located at the rear of the driver. The entire driver housing and horn structure is constructed of molded plastic. The outer diameter of the cone is clamped in a plastic flange and the "back volume" is created by a thin plastic dome or cap mated to this same flange.

Measurements shown later indicate that this back cap and flange had a high quality factor resonance near the fundamental resonant frequency of the PZT disk. During transmission, the volume velocity from the cone excites the cap, and well after the transmission is finished, the ringing of the cap and flange impart a volume velocity onto the cone and PZT disk.

Because of the vibration of the back plastic cap, the transient response of the transducer was degraded. The transducer ringing following the transmitted pulse becomes longer and larger than that of an ideal one. It especially degrades the quality of the received signal at close range.

In order to understand the vibration of the plastic driver structure (Figure 12), "tap testing" was first performed by Hofler. A 12 mm B&K condenser microphone placed 3 to 5 cm from the bullet nose tip of driver horn (point B of Figure 12). The SR785 FFT analyzer analyzed microphone signals over a frequency span of 0-6400 Hz. Two different CTS drivers were measured in this testing. One was an unmodified driver and the other was modified by removing the paper cone and piezo disk. The solder holes were filled with solder and sealed. The driver horn was either gently held in fingertips from the corners of the horn face, or gripped tightly in the palm around the back cap.
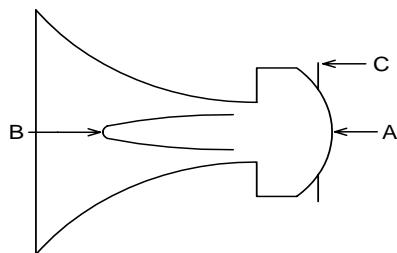


Figure 12.        Vibration resonance of plastic driver structure.

A variety of tap testing experiments were conducted for the unmodified and modified drivers, respectively. Two sets of testing items of driver housing are listed in table below.

| Driver | Item | Testing content |
|---|---|---|
| **Unmodified** | 1 | Tapping (small Allen wrench) on front bullet nose, point B. |
| | 2 | Plucking metal tab at point C. |
| | 3 | Tapping on back cap on center, point A. |
| | 4 | Tapping on front bullet nose, point B, with larger Phillips screwdriver. |
| | 5 | Same as above #4, but clutching the backside of driver tightly in hand. |
| **Modified** | 1 | Tapping on back cap on center, point A. |
| | 2 | Plucking metal tab at point C. |
| | 3 | Tapping on nose, point B. |
| | 4 | 3 averages of tapping on noise, point B, while clutching backside in hand. |
| | 5 | Same as above, no averaging. |
| | 6 | Tapping on back cap on center with fingernail. |

Table 1.    Tap testing of driver housing

Figure 13 below shows the direct microphone waveform.  It is obvious that the empty driver housing has a significant resonance. Figure 14 shows the frequency response of the same signal. There are strong peaks at 2700 and 3000 Hz and two weaker peaks near 4000 and 5300 Hz.

The empty driver housing is a nice testing platform because resonances of the piezo disk or the disk and paper cone combination are excluded.  However, this may alter the resonant frequency.

3 ms/division
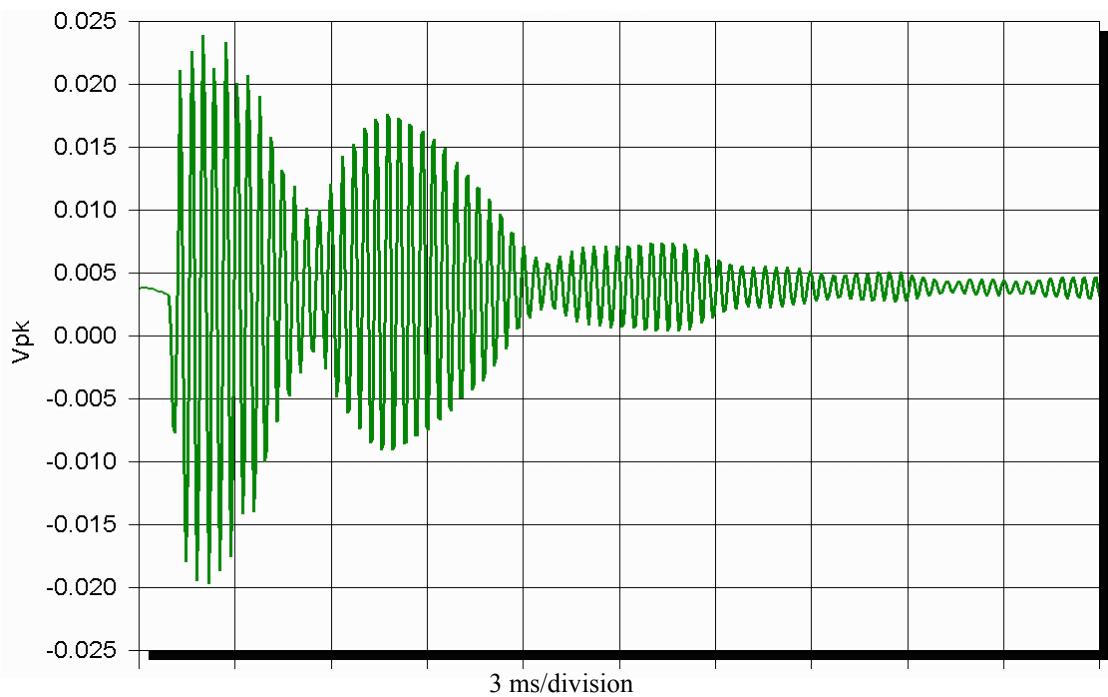
Figure 13.        Microphone waveform after plucking the metal tab at point C, for "empty" modified driver.
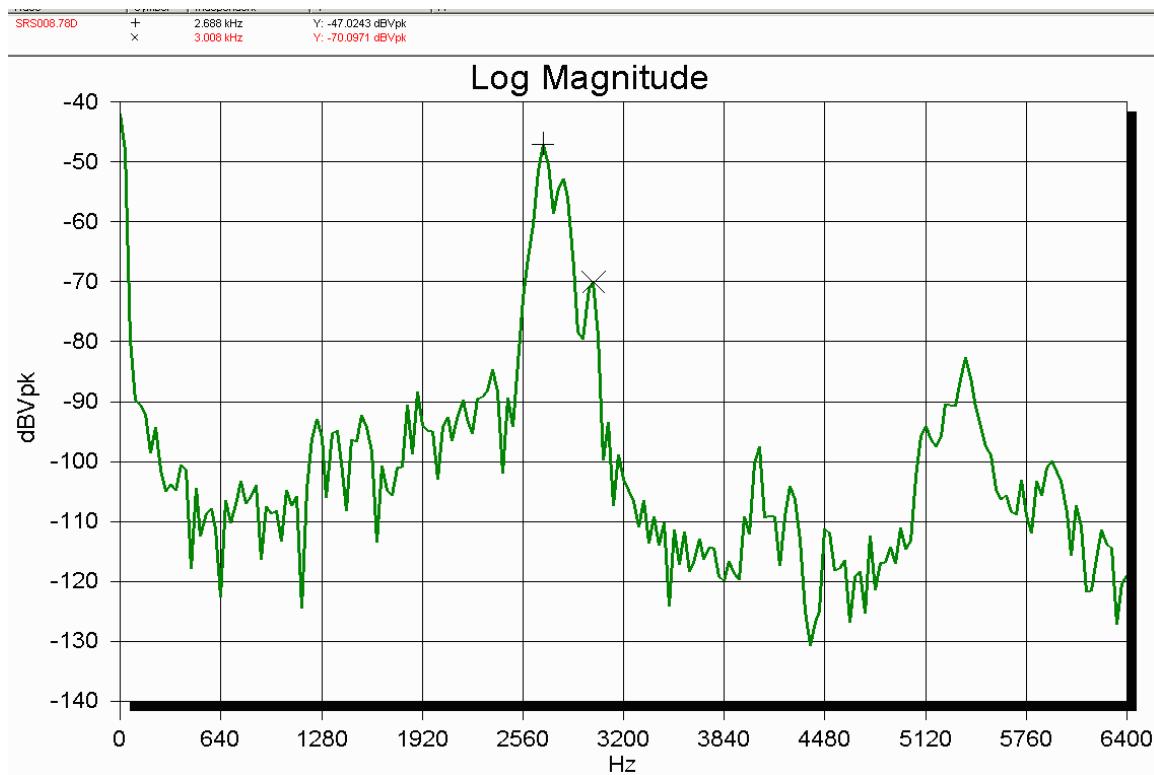


Figure 14.        FFT of previous microphone waveform.  Note strong peaks at 2700 and 3000 Hz and two weaker peaks near 4000 and 5300 Hz.

23

Figure 15 below shows the result of tightly gripping the back plastic cap in the hand to damp the resonances, for the unmodified driver unit. Figure 15 is very interesting for two reasons: 1) There is a strong resonance at 3550 Hz in the no damping case. This is important because it lies very near the desired frequency of array operation. 2) In the damped case this peak mostly disappears. It would appear that the solution to our problem is to apply mechanical damping material to the back plastic cap and metal tabs.
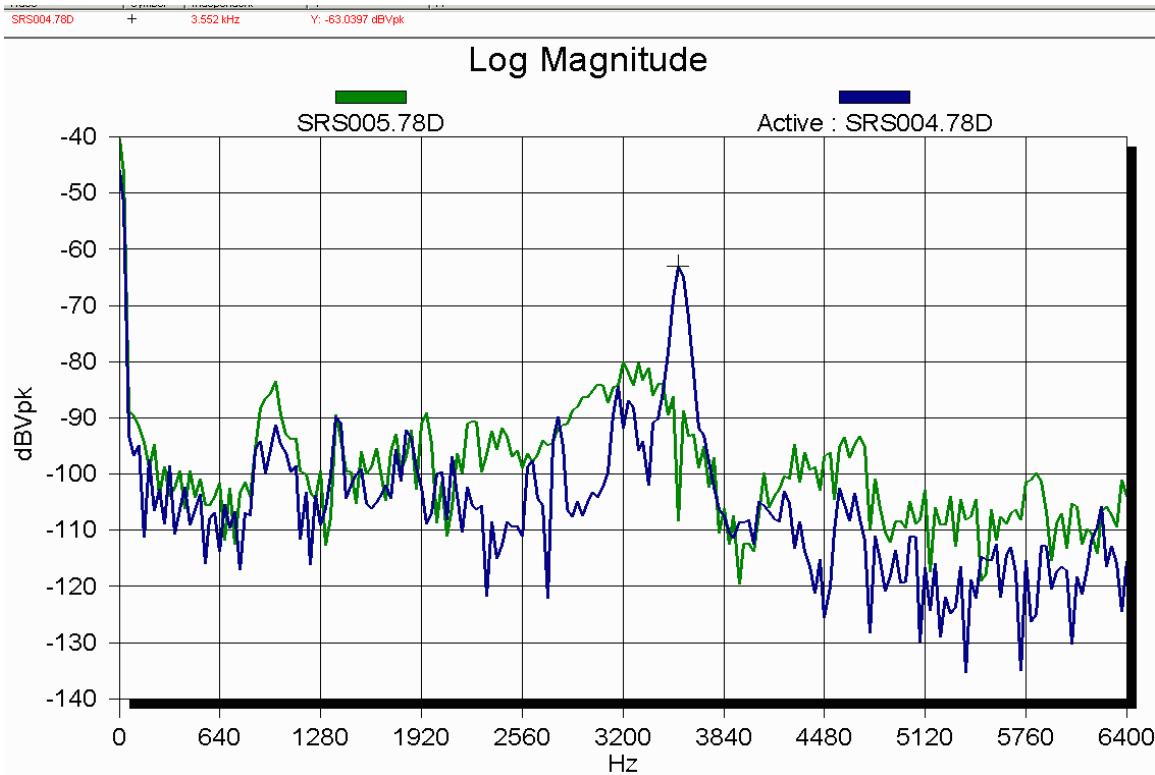


Figure 15.　　Power spectra of unmodified driver. Blue curve: tapping on the front bullet nose, point B. Green trace: the same as blue, except the back cap was gripped tightly in hand. Note suppression of strong peak at 3550 Hz.

## C.　SINGLE DRIVER TESTING

A test circuit similar to the one shown in Figure 11 was used for transient testing in the anechoic chamber. The driver had 15 mH tuning inductor in parallel and was coupled to the LT1028 via a 220Ω resistor with a 2K resistive shunt to ground. It was positioned in the anechoic chamber floor on a piece of foam, pointed upward. The first driver used is the standard CTS unit with some white Eberhard-Faber brand modeling

clay applied to the plastic back cap and around the screw flange (Figure 16). The clay was also pushed into the region of the metal tab attachment points, to damp the flexural resonances of the tabs.
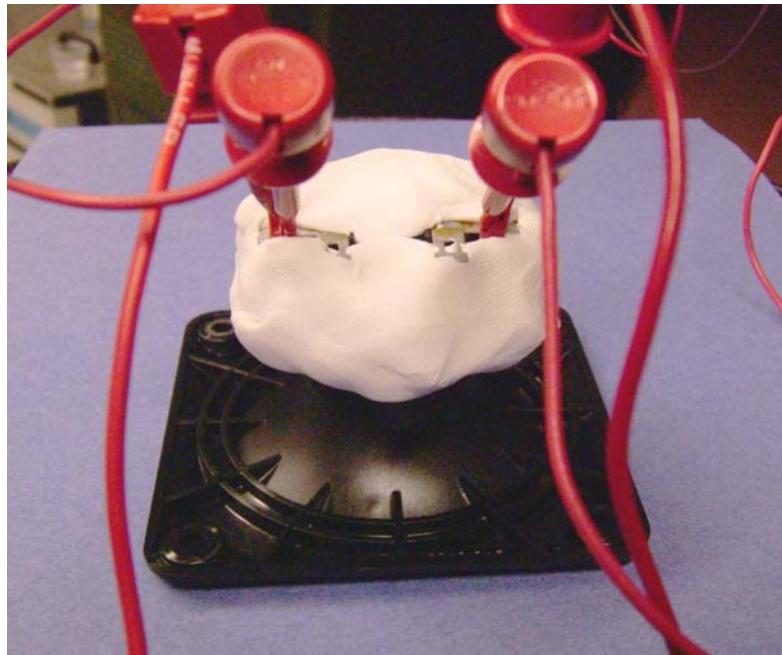


Figure 16.        White modeling clay covering back cap and metal tabs.


All of the testing done around this time frame used a transmitted tone burst signal of 3600 Hz where the receiving sensitivity is quite high with a tuning inductor. Later, it was discovered that the transmission efficiency of the driver was considerably better in the frequency range from 4100 to 4300 Hz which was probably better for all-around sonar performance.

The general settings of the equipment were: preamp voltage gain = 100; 6 cycle burst at 3600 Hz; 7.0 $V_{pk}$ drive; 15mH parallel tuning inductor; no switched damping resistor. The first reflection objects were the lights and the motor rotator in the anechoic chamber, which typically showed up on the scope trace at a round trip transit time of roughly 14 ms.

Figure 17 and 18 show the output signal for both driver units with and without modeling clay attaching to the plastic back cap. It is quite apparent that the modeling clay

greatly damps the ringing of the plastic back cap. Additionally, the effect of the clay attached to the plastic back cap can also be seen clearly in the electrical impedance data of the driver as shown in Figure 18.
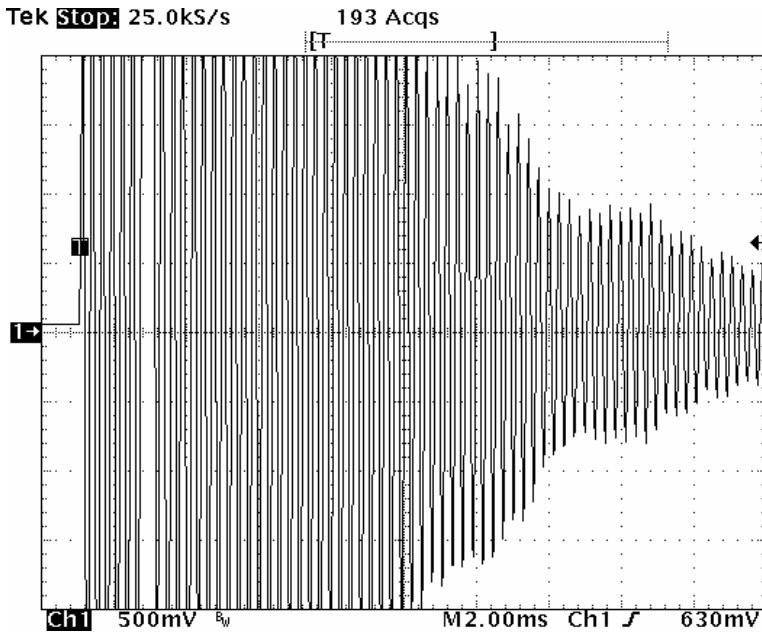


Figure 17.  Unmodified driver without damping clay. Ringing of the plastic back cap is massive at 3600 Hz.
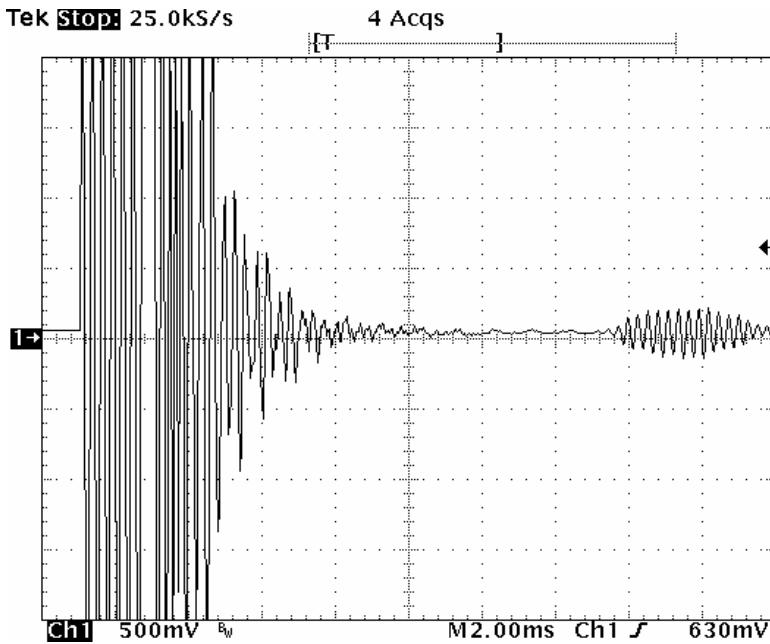


Figure 18.  Test conditions are identical to Figure 17, except the driver has its plastic back cap damped with white modeling clay. First return in anechoic chamber at a distance of about 2.5m is visible.

Figure 19 shows the impedance of an unmodified driver and we can see the odd peak shapes. Figure 20 shows the impedance of a driver with clay and the curve looks like the simple theory.
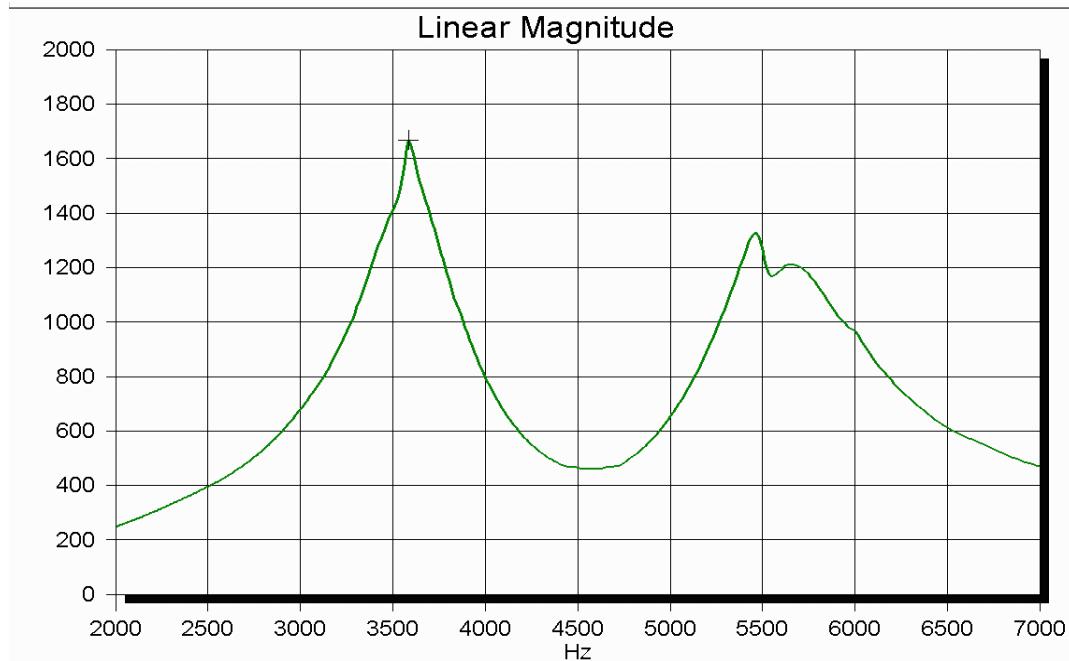


Figure 19.      Impedance of an unmodified driver with a parallel tuning inductor in the anechoic chamber. Vertical scale is in Ohms.
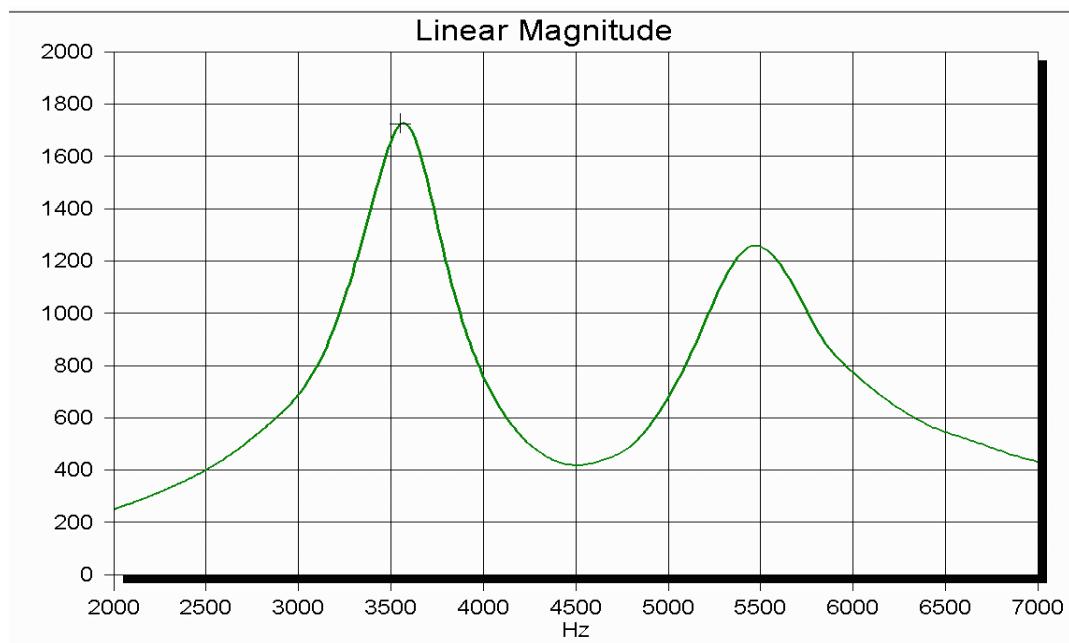


Figure 20.      Impedance with white modeling clay applied to back plastic cap.

### D. ARRAY #2 MEASUREMENTS

#### 1. Received Signal of Unmodified Array

We measured the admittance or conductance peaks of 42 different CTS brand, model KSN1167 drivers. The frequency of the peak center of the conductance was measured with clay added to the backside of the driver unit, with the driver placed in the anechoic chamber. The frequency of the peak center of the measured conductance (or G = Re Y) data should reflect the resonant frequency of the mechanical resonance of the piezoceramic flex disk used as the transduction element in the driver. The 19 drivers of array #2 were selected from the above 42 measured ones. A group of 19 drivers having the closest values of $f_s$ resonant frequencies and $G_{MAX}$ peak heights and were connected in parallel.

The array was laid on a piece of foam on the bottom of the anechoic chamber pointing straight up. The T/R circuit is the Hofler circuit shown in Figure 11, with the receiver preamp having a voltage gain of 100. The transmitted signal conditions were: 6-cycle square burst at 4110 Hz (G peak center); 7.0 $V_{pk}$ drive. Figure 21 shows the received signal from the unmodified array without any intentional reflector or tuning inductor.
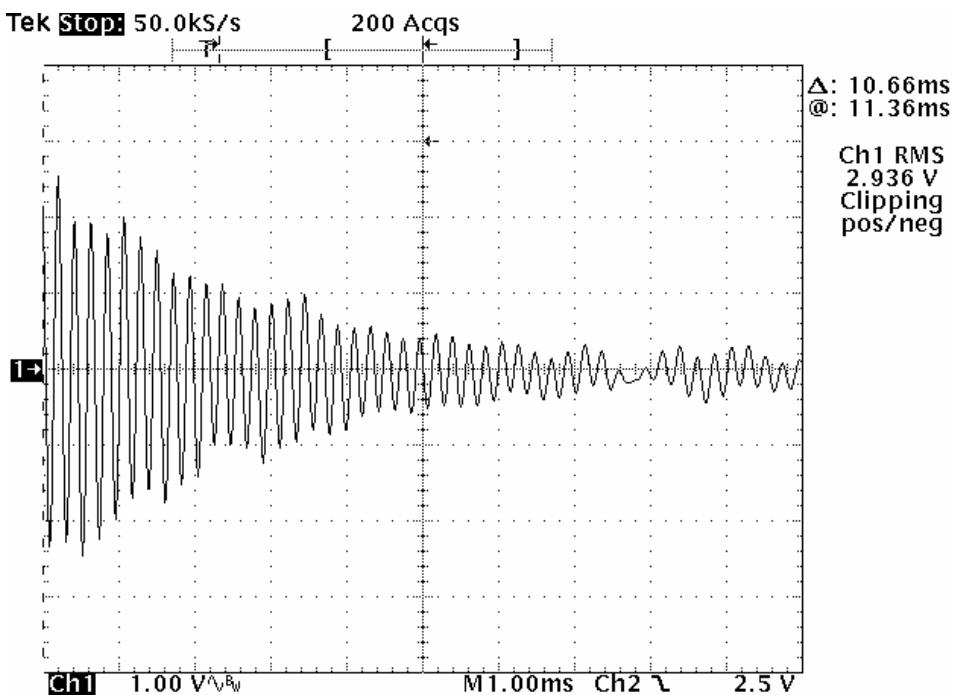


Figure 21.    Received signal without reflector at 4110 Hz (G peak center).

Figure 22 shows the received signal of unmodified array with a solid 76 mm aluminum sphere suspended above the array. The distance from the array box top to the sphere was 1.8m.
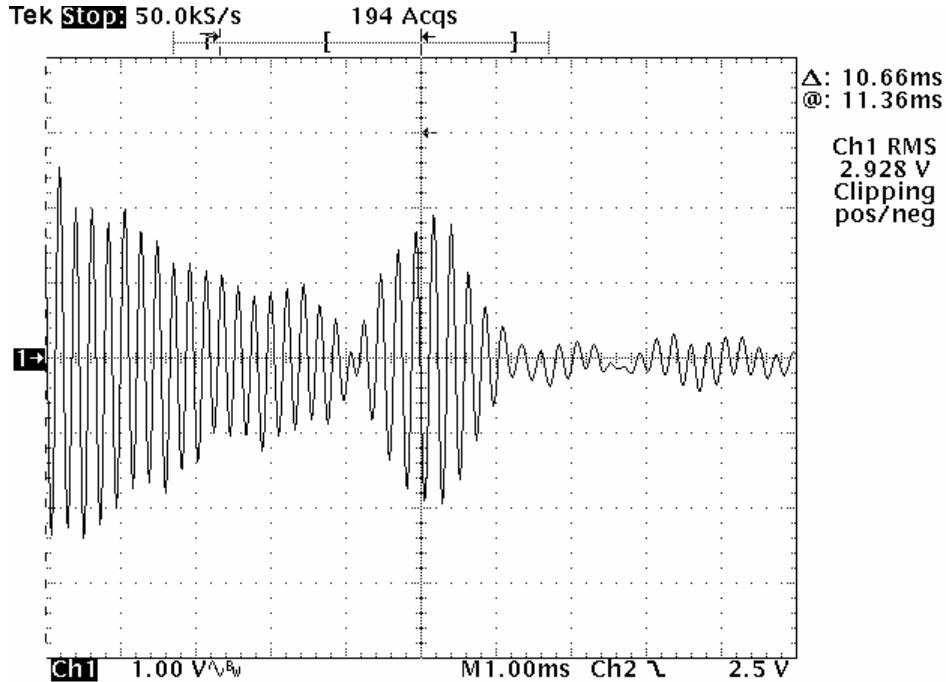


Figure 22.        Received signal with 76 mm spherical target at 4110 Hz (G peak center).

To conveniently compare the received signal, both of the above pictures have a 10.66 ms delay positioned at the center of the scope display due to the fact that the signal propagation distance is twice the separation from the array box top to the sphere. We also tried short Gaussian shaped bursts at 4230 Hz, and 4350 Hz, with and without the inductor. Generally, there were no surprises, with the narrower bandwidth of the Gaussian shaped bursts exhibiting slightly less spurious ringing.

### 2.        Acoustic Standing Waves

When two waves with the same amplitude and wavelength travel in opposite directions, their interference with each other produces a standing wave. If the standing wave volume is bounded by two relatively rigid surfaces at either end, the frequency of the standing wave is given by

$$f = \frac{nc}{2d}, \quad n = 1,2,3\ldots\ldots \tag{9}$$

where $c$ is the sound speed and $d$ is the separation between two boundaries where the waves oscillate.

There are two potential spaces where the phenomenon of the standing wave exists. One is in the interspaces between the back of the horn mouth and the top surface of the box and the other is inside the box. Here, we assume the back of the driver is perfectly enclosed, so that only a little sound energy could leak into the box; thus the influence of standing wave inside the box can be neglected. On the other hand, the effect of a standing wave reflecting from the top surface of the box is significant.

When part of wave from the standing wave combines with the directly radiated wave, they destructively interfere with each other so the amplitude of the resultant wave around frequency of 4650 Hz is less than original one. Figure 23 below shows the frequency response of a previous array measured by Walters. It is seen from this figure that a deep valley appears around a frequency of 4650 Hz. The narrow notch suggests a resonance with a Q of 30. At the time this was assumed to be an internal resonance within the transducer.
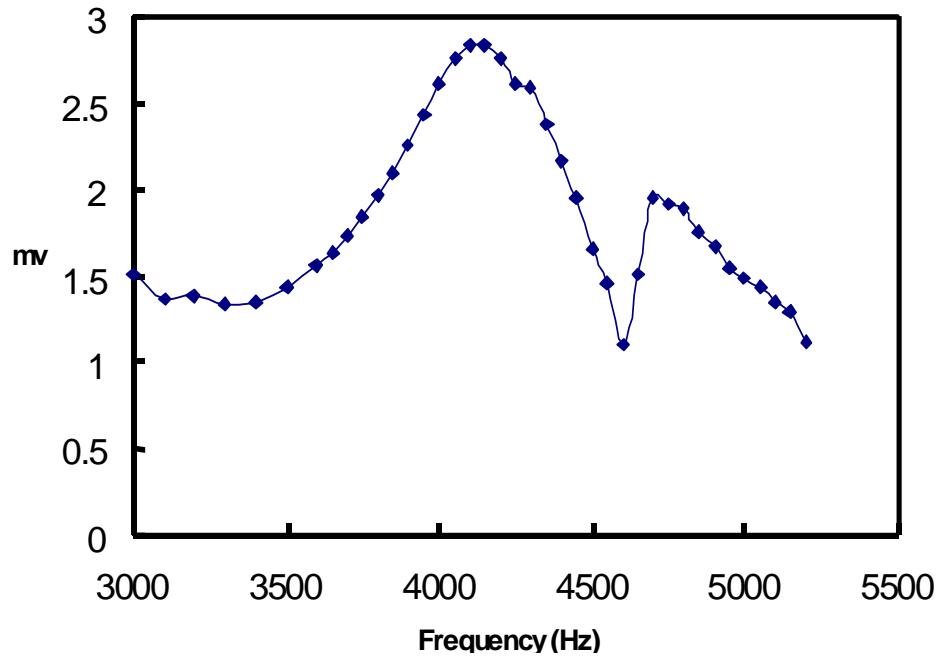


Figure 23.　　Transmitted frequency response of previous array measured by Walters.

The source of the ~4500 Hz ringing of the array was not apparent, and the frequency of the decaying pulse seen in Figure 20 was not the 3500 Hz resonance associated with the plastic transducer housing. It was possible that an acoustic standing wave existed between the flared horns and the top surface of the mounting surface. To determine if this was the case we placed a B&K 6 mm microphone into the interstitial spaces between driver horns of array #2 to measure the amplitude of the sound pressure. The microphone was placed at two different positions, roughly 5 cm inward from the perimeter of the array without making contact with the plastic drivers or the aluminum box. One position was near the center of the vertical extent of the interstitial space and the other was near the bottom of this space near the box surface. Figure 24 shows the spectrum of the microphone at the different positions. It is quite clear that there is a strong peak at about 4600 Hz.
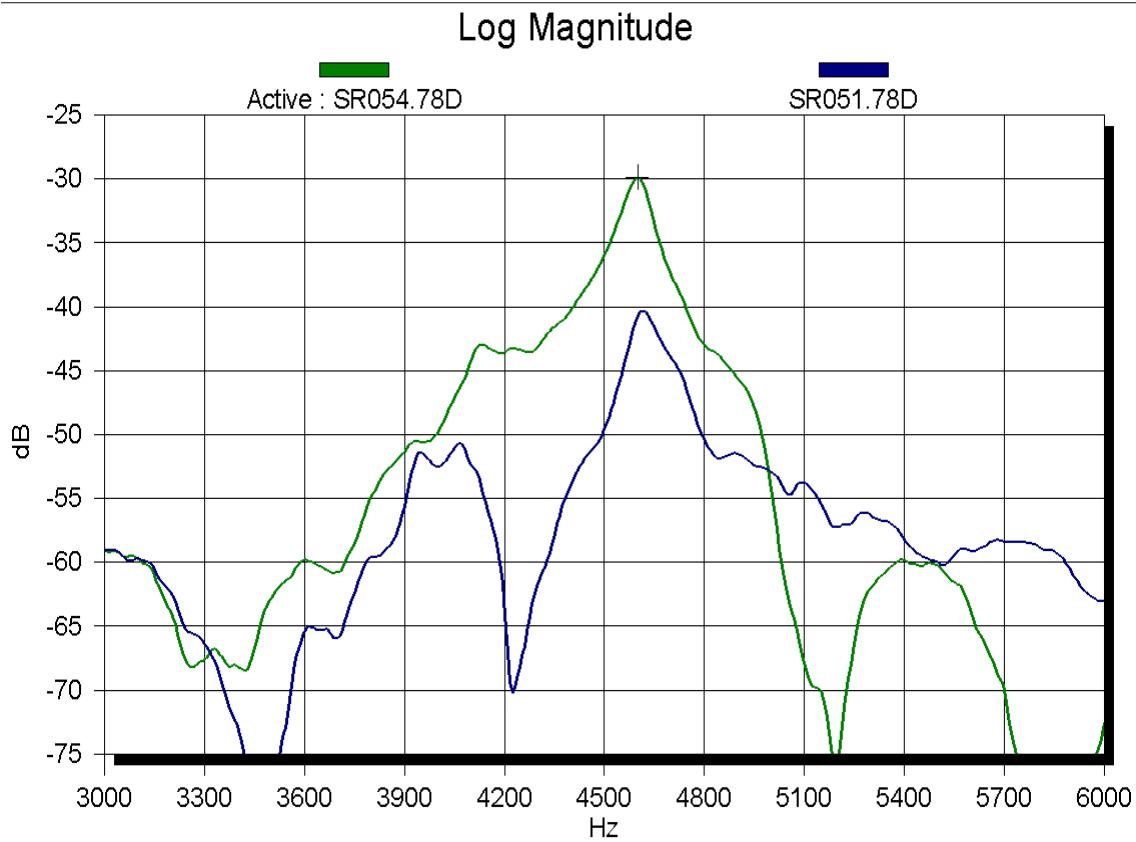


Figure 24.        Microphone signal from two positions in the interstitials spaces between horns in array.  Strong peaks are visible at about 4600 Hz.

31

Additionally, a transmitting response measurement was also conducted. In this measurement, a B&K 6 mm microphone was positioned above the array at 1 meter. The result (Figure 25) shows a deep notch located at 4630 Hz, which corresponds to the frequency of the peak in Figure 24 and was also seen in Figure 23 for an earlier array. The separation $d$ between the mounting plate and the driver horn was about 3.8cm and the sound speed c was 345 m/s (room temperature). Using Equation (9), the resulting fundamental resonance frequency is around 4540 Hz. This frequency is similar to the 4600 Hz standing wave seen in Figure 24. It is clear that destructive interference occurs between the outgoing radiation and the standing wave and creates a notch.
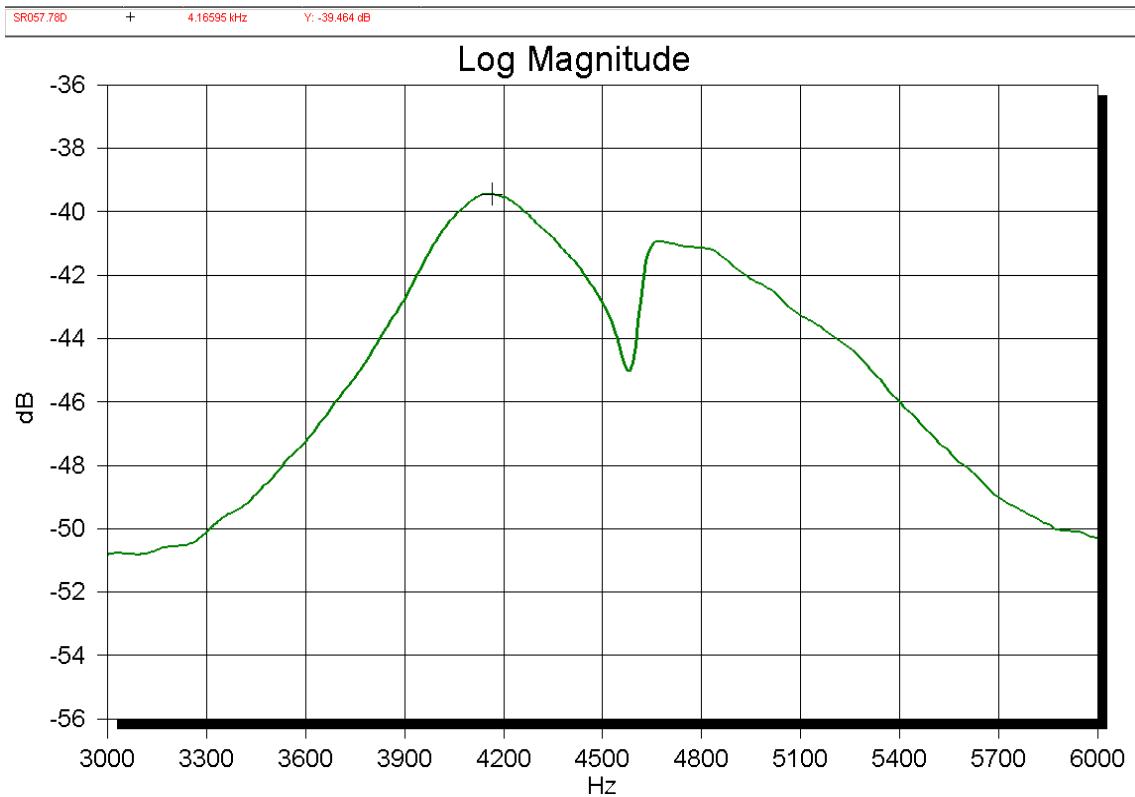


Figure 25.        Anechoic transmitting voltage response of array with 6 mm B&K at 1m.

To reduce the interference effects of the standing wave, we first sealed the cracks between the mouths of the driver horns with clay (Figure 26) and then performed the same TVR measurement.  Later, we wrapped the perimeter of the array of horns with a strip of foam rubber (Figure 27). The foam strip has a cross section of 4.6 cm square and

it was fastened in place with a double wrap of cotton string. The foam was forced into the gap between the horn flange and the aluminum top plate, so the seal should be reasonably good. Again, the same transmitting response measurement was made.



Figure 26.       Array #2 with interstitial spaces between horns shown as well as the modeling clays used to seal the small gaps between the mouths of the horns.



Figure 27.       Array #2 wrapped with foam rubber to seal and damp interstitial horn space from the outside.

Figure 28 below shows the transmitting response of array #2 before and after modification. We can note that most of the improvement is achieved with the modeling clay sealing the horn gaps at the front of the array. However, there is still a small but measurable effect at 4640 Hz that is eliminated when foam is wrapped around the perimeter.
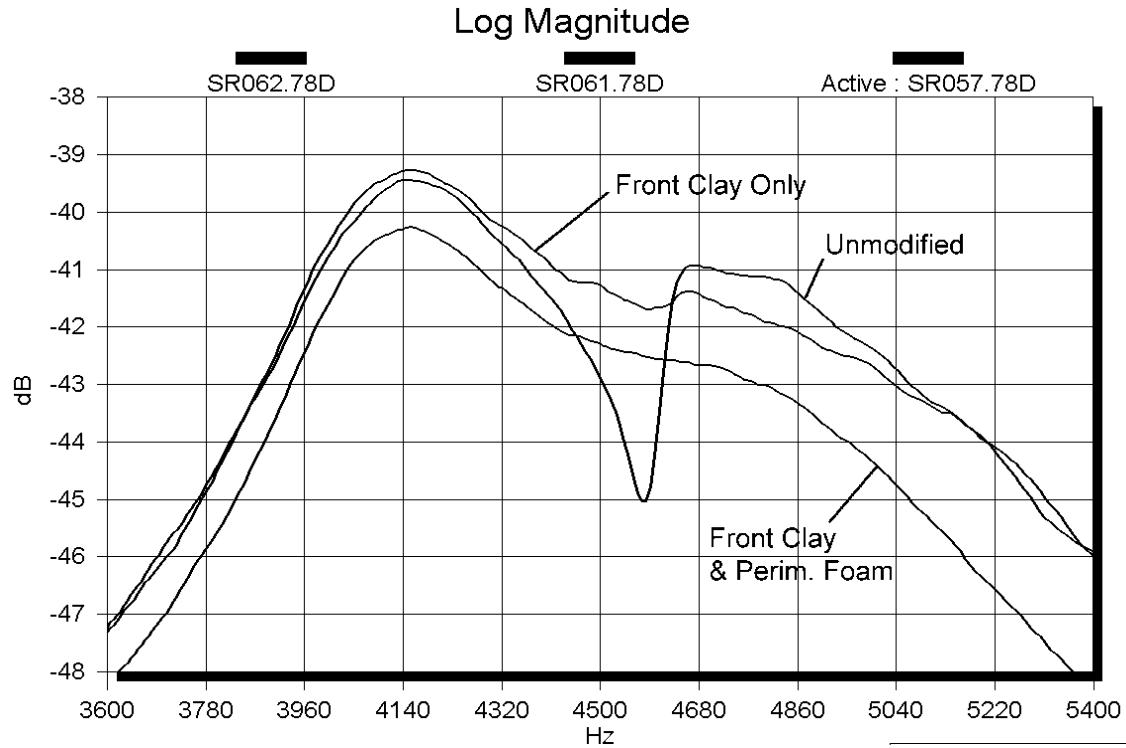


Figure 28.        Array #2 TVRs before and after modifications.

### 3.        Received Signal of Modified Array

Finally, we re-measured the received signal from the array after modification and compared the differences with that of an unmodified array. The transmitting signal had a gaussian shaped tone burst at 4120 Hz and without inductor connected in parallel to the pre-amplifier.

Figure 29 first shows the received signal of unmodified array #2 with a 76 mm aluminum sphere suspended above the array.

34
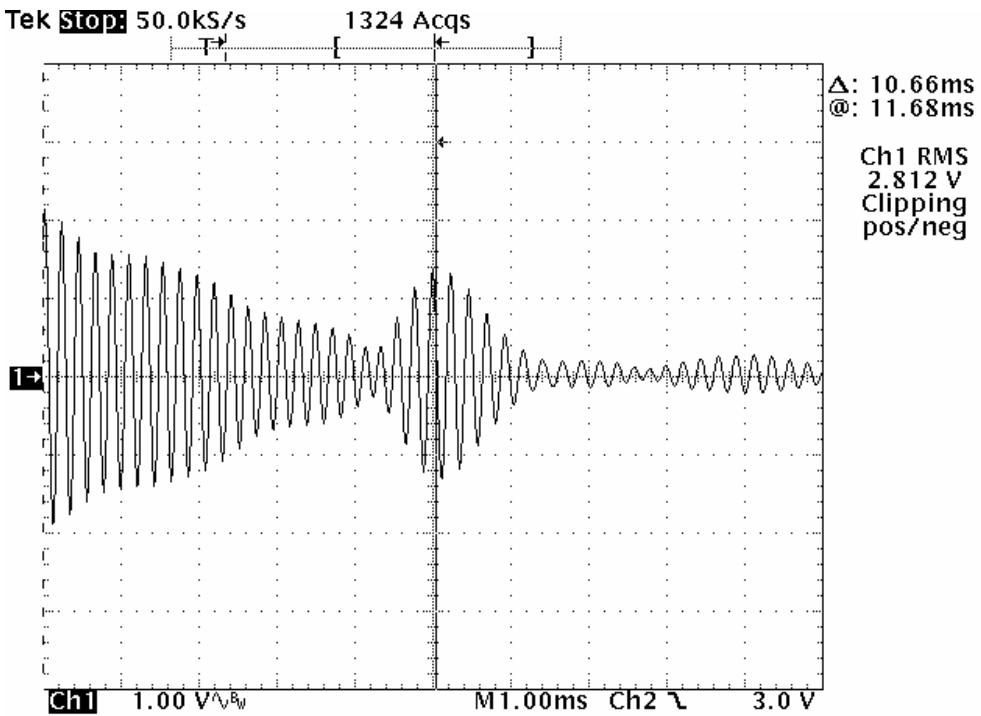
Figure 29.      Received signal of unmodified array #2. Transmitting and receiving a gaussian shaped tone burst at 4120 Hz with 76 mm reflector sphere, no inductor.

Figure 30 shows the received signal of array #2 modified with front clay and perimeter foam. The display was enlarged with 2 times higher vertical sensitivity. The ringing on the left side of the waveform was dramatically reduced. Figure 31 is the same test as the previous one but with further refinement. The array #2 fully was modified with front clay, perimeter foam, and clay on the back plastic caps of the 19 drivers. An even larger reduction in ringing on the left side of the waveform occurred.
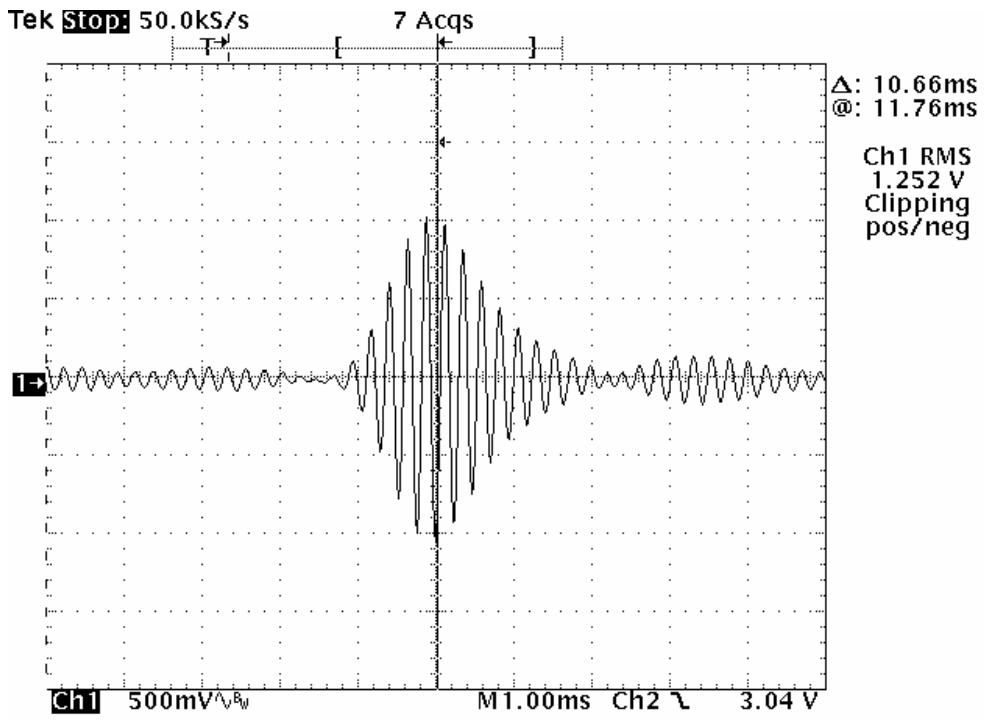
Figure 30.        Received signal of array #2 modified with front clay and perimeter foam.
Note the 2X higher vertical sensitivity.
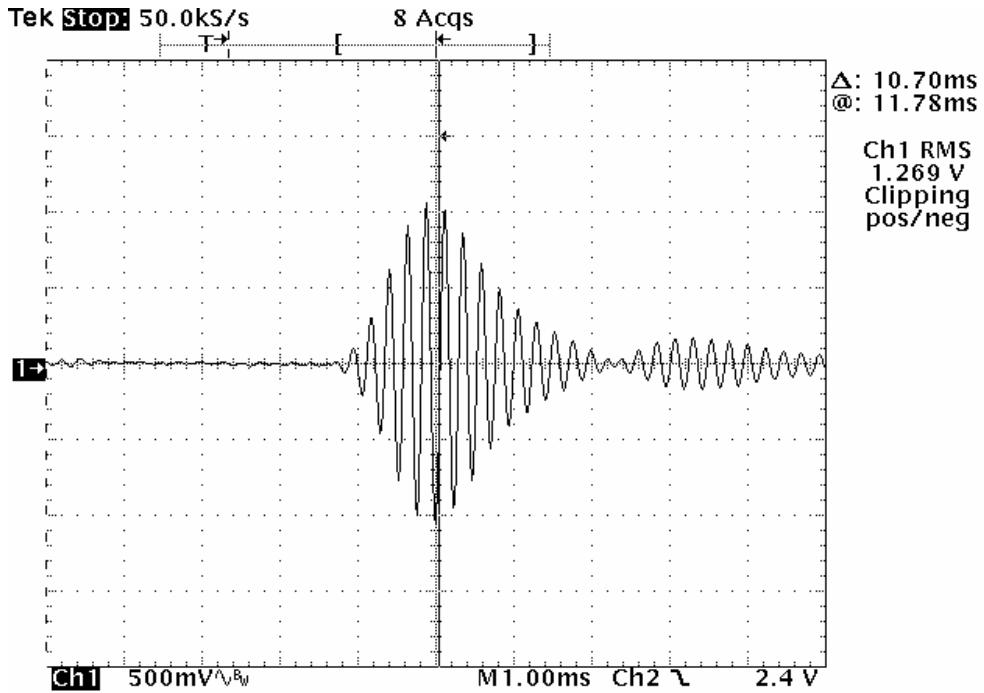


Figure 31.        Received signal of array #2 modified with front clay, perimeter foam, and
clay on the back caps.

Figure 32 is the same as previous one, but with 2 times vertical sensitivity and a time shift. Comparing with Figure 29, the received signal of the unmodified array, we can note that the residual signal at around a 9 ms delay point decreases from 0.7 $V_{pk}$ to 15 $mV_{pk}$, that is, the reduction in ringing at this point is about −33.4 dB. Filling the spaces between the drivers, using foam to surround the array and using clay on the back side of the plastic housing was quite effective in reducing the residual ringing.
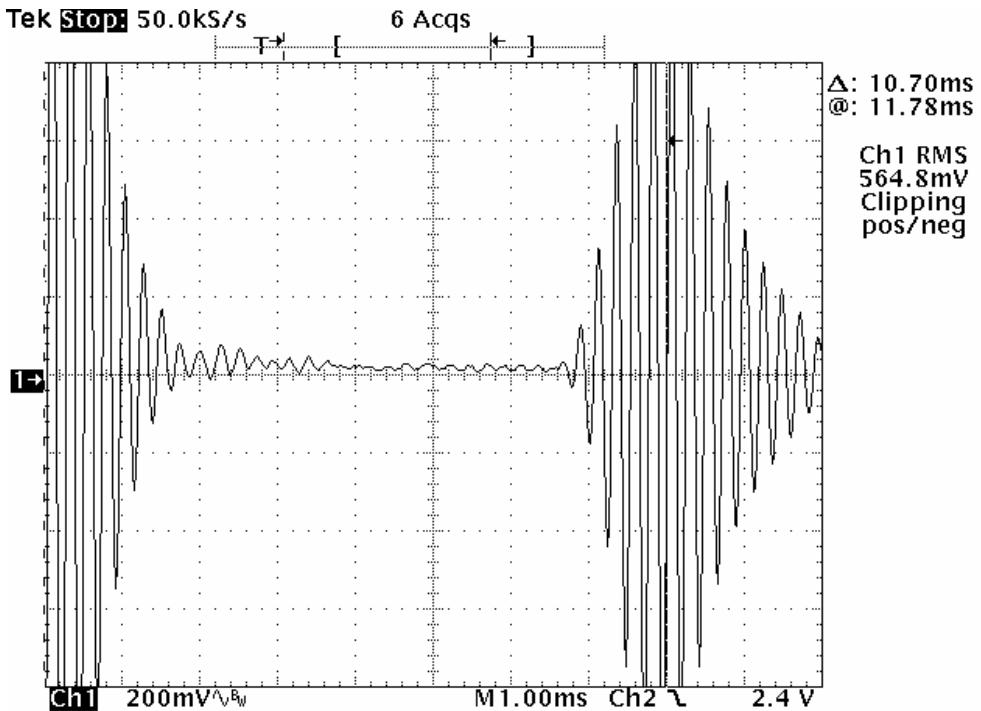


Figure 32.        Received signal of array #2 modified with front clay, perimeter foam, and clay on the back caps. Note the further 2.5X increase in vertical sensitivity.

The next step involved connecting a 790 uH tuning inductor, which increased the receiving sensitivity. As discussed in preceding chapter, adding a parallel inductor would increase RVS sensitivity. Figure 33 below shows the measured result, and as expected, when compared to Figure 31 it demonstrates that a 4 dB increase occurred in the RVS by adding a parallel inductor.
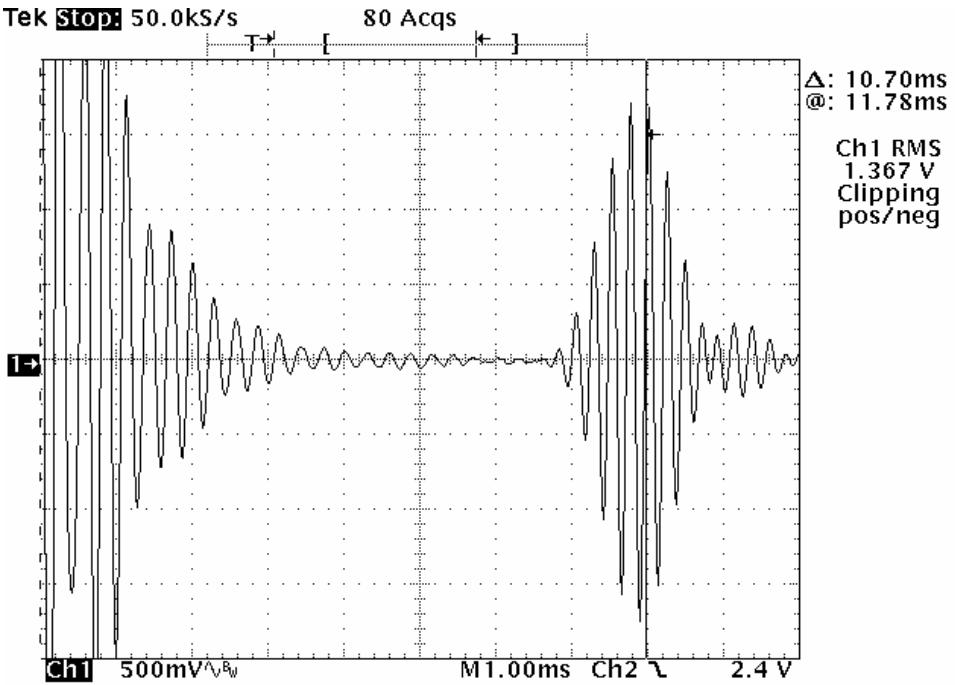
Figure 33.　　The same test as the previous two figures, except the array was electrically loaded with a parallel tuning inductor.  Note that the 10.7 ms delay point has been shifted from the center of the figure to the right.

## E.　FIELD MEASUREMENTS

Field measurements were preformed on the roof of the Spanagel Hall. The purpose of the measurement was to show how well the modified array improved the performance. Figure 34 shows a plot of the magnitude of $C_T^2$ represented in terms of intensity with the Doppler frequencies of $\pm$ 4 m/s as color and it was taken on March 2002, 10:07:38 UTC (night) Starfire Optical Range, New Mexico, with an early hexagonal array. The deep red regions mean air moving away from the acoustic echosounder, the green regions have zero vertical motion, and the deep blue regions are air moving close to the acoustic echosounder. The strength of the turbulence determines the brightness of the color.

The region between 0 m and 15 m at the bottom of Figure 34, a blue stripe, was useless because the transducer ringing degraded the received signal. Figure 35 shows the profile of the array #2 without a tuning inductor, and it was taken on 11 October 2004

17:00 (PDT), at NPS. It is quite clear that the bottom band due to the transducer ringing was reduced significantly from 15 m to 5 m.
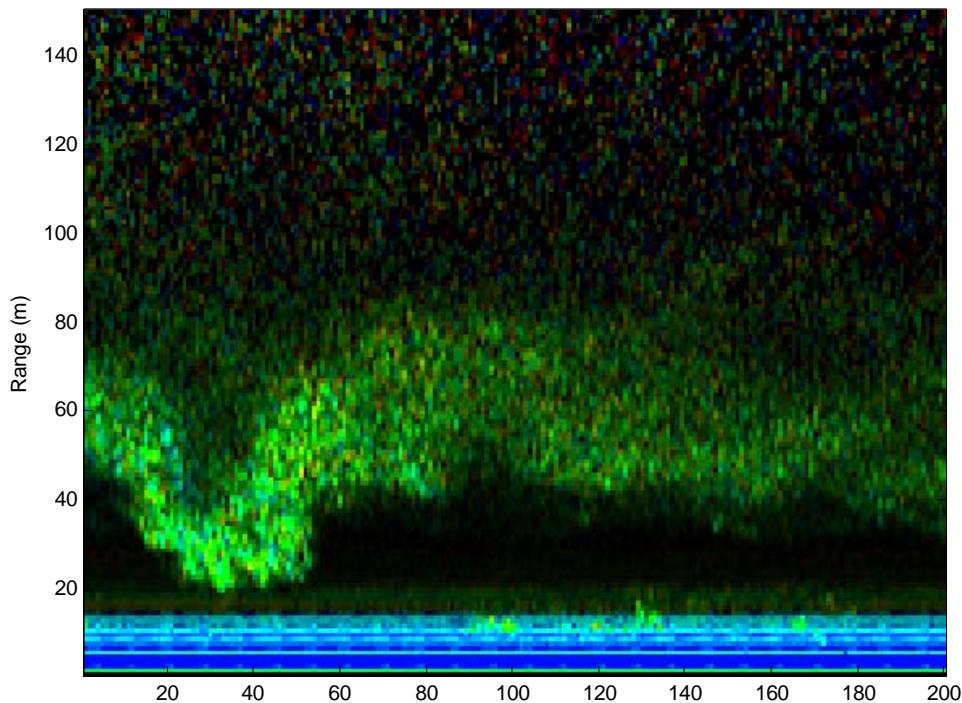


Figure 34.        Atmospheric Turbulence within the first 150 m. Note the 0-15 m transducer ringing (from Walters).
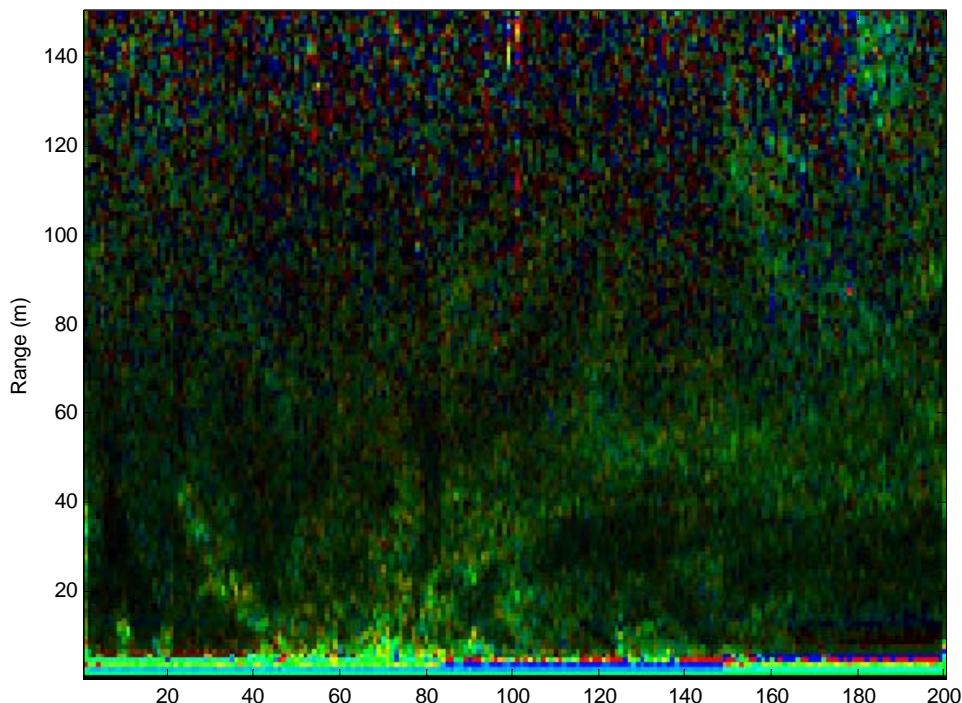


Figure 35.        Profile of modified echosounder (array #2). Note the reduced transducer ringing.

Figure 36 shows the same test of array #2 with and without a parallel tuning inductor. The data at the left side of the display was the reflect signal without the inductor, and that at the right side is the signal is with a 790 uH tuning inductor. Since the strength of the signal appears as brightness, the right side of the plot shows that the inductor increased the transmit-receive sensitivity of the acoustic echosounder substantially.
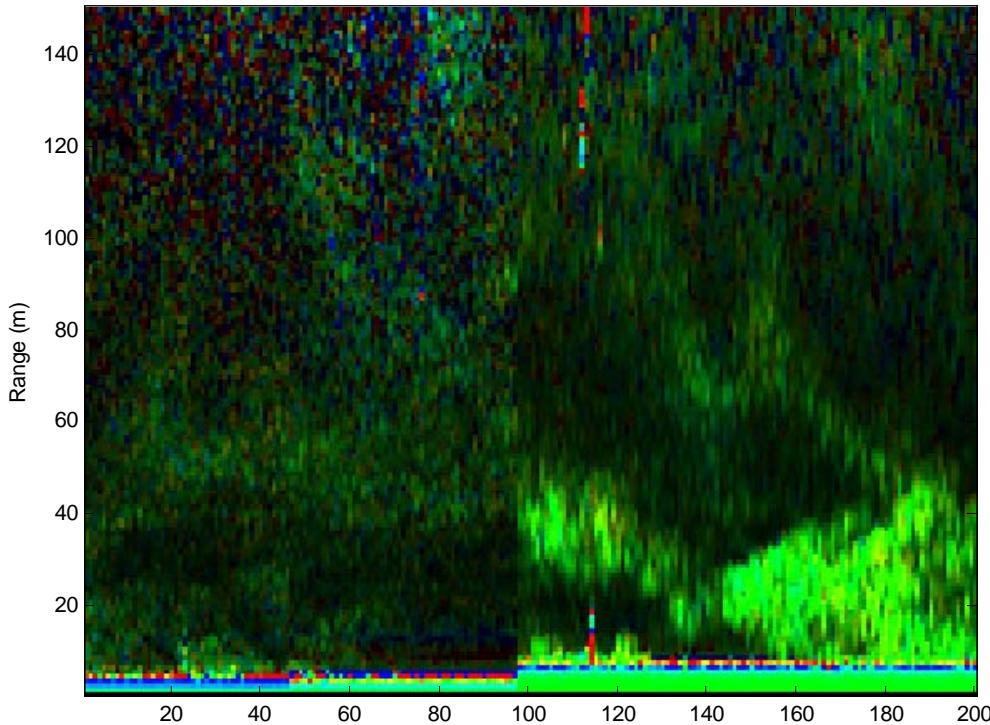


Figure 36.        Same test with Array #2, with no inductor and with 790 uH inductor after 98 seconds.

## F.        ARRAY CONFIGURATION IMPROVEMENTS
### 1.        Building Array #3

To effectively eliminate the interference influences of the standing wave from the interstitial spaces between the back of the horn mouth and the top surface of the array box as well as the vibration from the back plastic cap of the driver, we built a new array #3. The mounting box was constructed of sheet aluminum and its height was tall enough to enclosed a sheet of 12 mm plywood board in the bottom of the box as a spacer, a 25 mm layer of lead lined urethane foam is placed on top of the plywood to absorb noise signals and vibrations, and the whole horn body of the driver. In addition, we selected another group of 19 new CTS drivers having the closest values of $f_s$ resonant frequencies and

G$_{\text{MAX}}$ peak heights in place of previous ones. The outer edge of every horn were cut to form a circular shape in order to place the drivers closer together. The horn mouth diameter was now machined to 75.7 mm and this diameter is raised about 6 mm above the surface of the array face plate. The horn mouths of the drivers were sealed to the front panel of the array box with silicon rubber and the back plastic caps of the drivers were pressed into the 25 mm foam layer to provide mechanical damping.

### 2.    Array #3 Measurements

The admittance measurement of the array #3 was conducted in the anechoic chamber with the exactly same experimental settings and procedure as that of array #2. Figure 37 compares the conductance of array #3 with that of fully modified array #2. It is seen that in addition to the main operating frequency peak at 4150 Hz, there exists another higher peak for array #3.
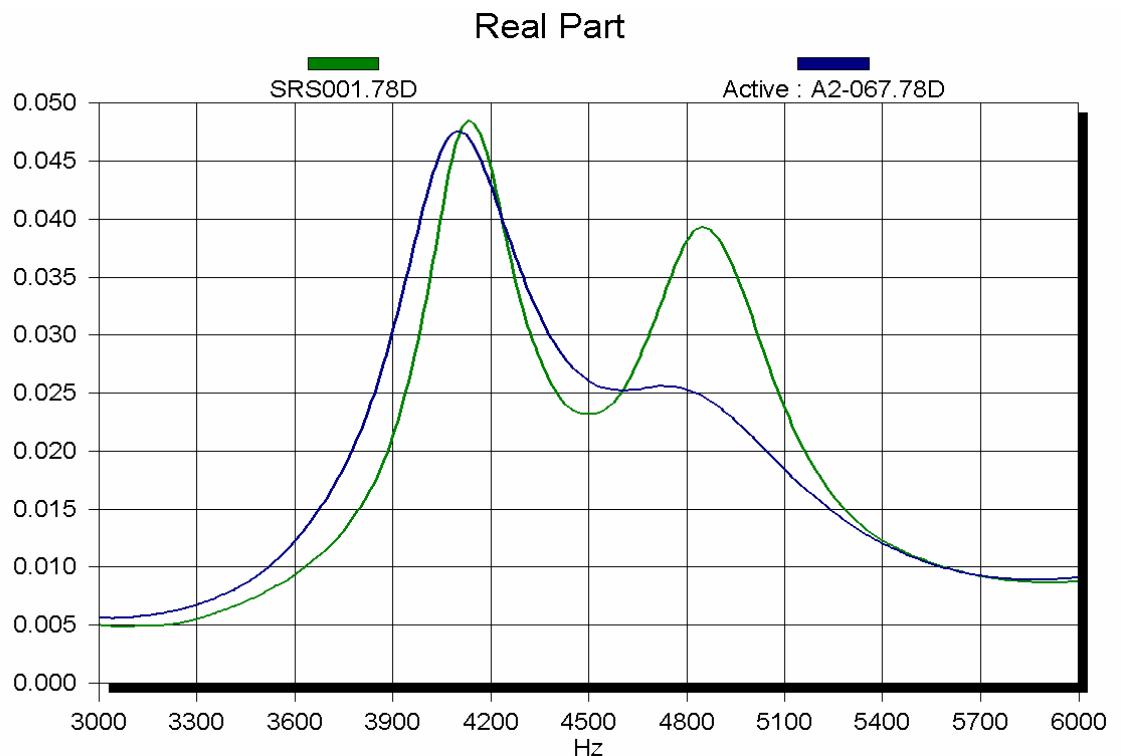


Figure 37.    Comparison of Array #2 fully modified and the new Array #3 with sealed horn mouths.  The real part of the admittance or conductance was measured in the anechoic chamber.  The vertical units are in Siemens.

To reduce the interference effects and diffraction from the edges of the circularly horns we filled the area between the horns with clay to make a flush front surface (Figure 38).



Figure 38.        Filling in the horn mouths of array #3 with clay to make a flush front surface.

Figure 39 below shows the comparison of TVRs measured with 6 mm B&K microphone, of the fully modified array #2, unmodified array #3, and array #3 modified with front side clay. It is noted that the on-axis TVR curve is consistently higher across the spectrum after modification.  Considerable acoustic energy must have been radiated off-axis for array #3 until the clay was added and the horns were effectively flush mounted.
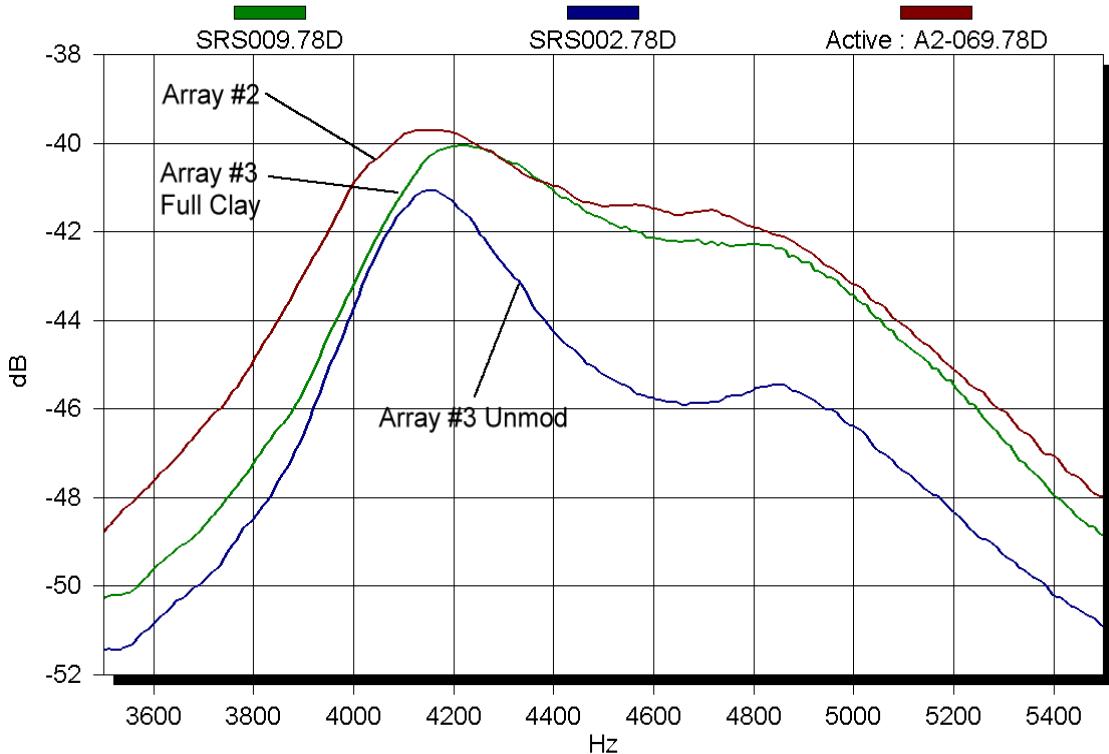
Figure 39.        TVRs measured with 6 mm B&K microphone, of fully modified Array #2, unmodified Array #3, and Array #3 modified with front side clay.

Figure 40 below shows the same type and strength of transmit/receive test as shown previously with the fully modified Array #2 (no inductor), except this test was performed with the clay modified Array #3. We can note that the ringing at left is moderately higher (worse) than the best data achieved with Array #2. The above data was taken with the back caps of the driver pressed into a layer of foam rubber.  Apparently, this is not as effective as attaching clay to the back caps.

The next step involved measuring the Receiving Voltage Sensitivity (RVS) of array #3. A 38 mm diameter soft dome tweeter was suspended from the ceiling of the anechoic chamber and directed horizontally. It's transmit response was measured (swept sine) with a 6 mm B&K microphone at a distance of about 63.5 cm. The tweeter response was not very flat because there was significant frequency response ripple. The ripple was reduced by taking 3 or 4 sweeps at different positions slightly off-axis at the same distance and averaging them.
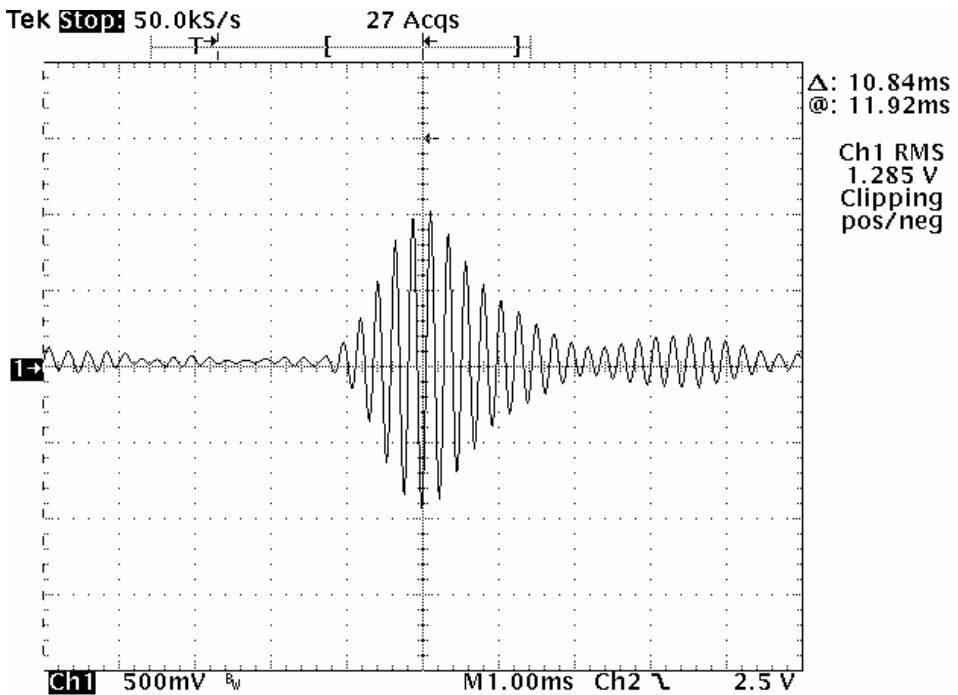
Figure 40.        Received signal of array #3 modified with front side clay.

Array #3 with full front clay treatment and the back caps pressed into the lead lined urethane foam was suspended at the same height as the tweeter sound source, and the receiving response of the array was measured with swept sine waves. These data were then corrected for the tweeter response later in software, to yield RVS response curves as in Figure 41. The three array conditions used were: 1) No electrical loading, called "No L"; 2) Loading with a parallel inductor called "L=790uH"; 3) Loading with a parallel LC combination with L = 135 uH, C = 8.2 uF which is called "// LC".

The relative curve heights of the 3 RVS curves used an arbitrary but common dB scale, so that they could be compared. Thus the "L=790u" curve is the most sensitive. TVR data had been taken earlier with Array #3. These data were used to compute TVR*RVS products (Figure 42) which should represent the round-trip transfer function for the acoustic echosounder.
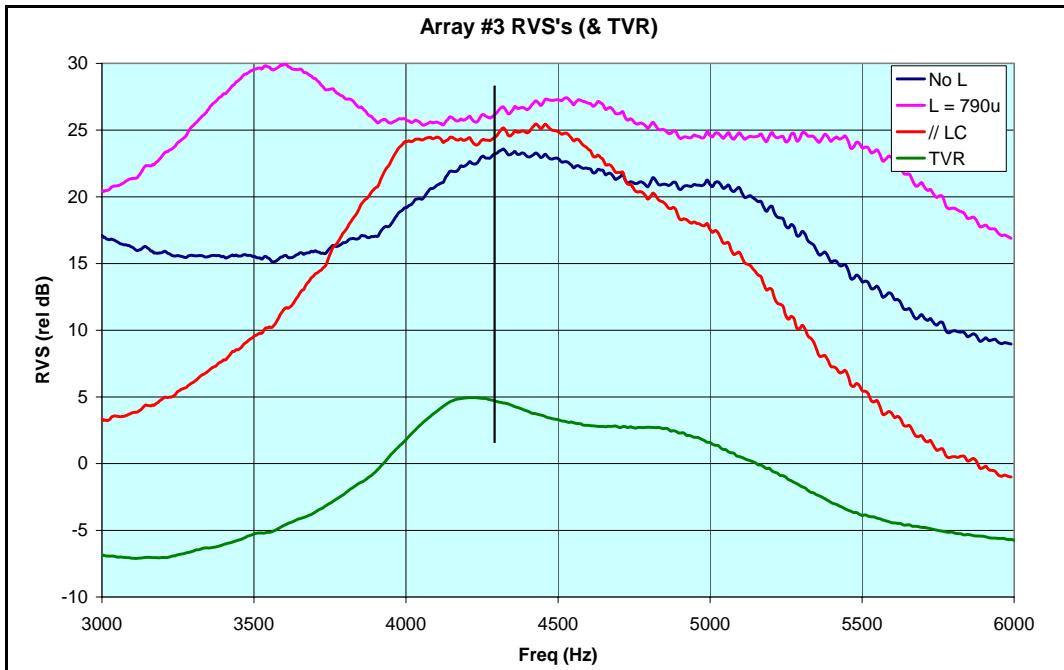
Figure 41.    Three RVS measurements for Array #3 with three different electrical loads: none, L=790uH, and an LC load with L=135uH and C=8.2uF. The TVR response is also plotted for comparison.  Note that the optimum operating frequency appears to be about 4280 Hz.
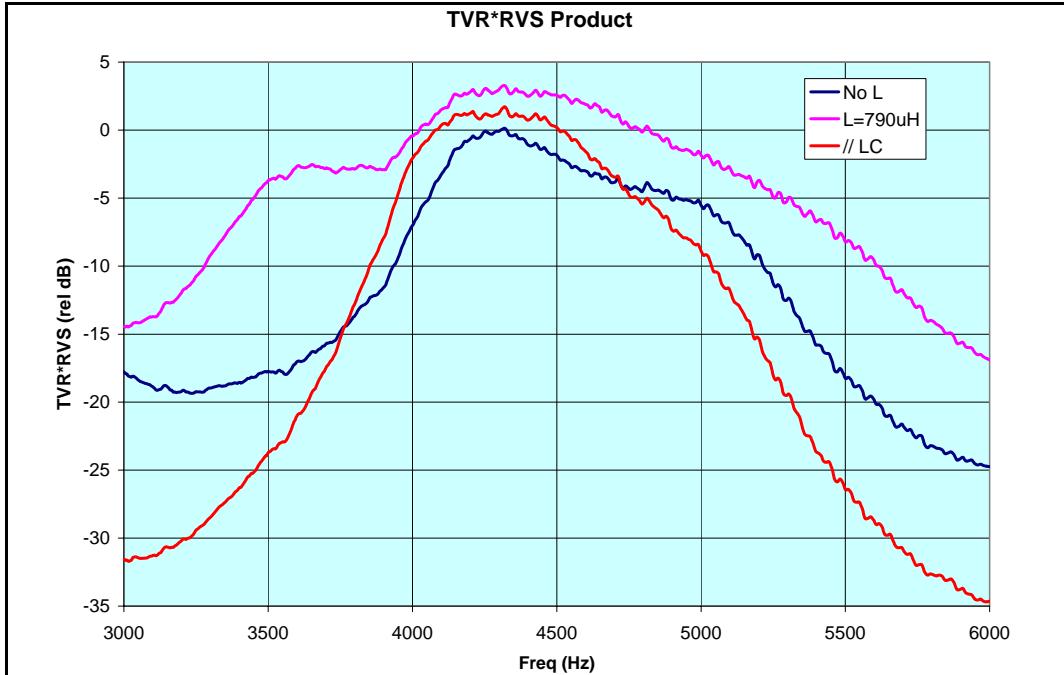


Figure 42.    Three RVS*TVR product response curves for the three different electrical loads used in the previous figure.  The response curves should illustrate the net transmit/receive response caused by the transduction, but ignoring any environmental or reflector response variations.

45

## G. SINGLE DRIVER TESTING OF BACK CAP DAMPING TREATMENTS

To mitigate the vibration effects of the drivers, array #3 has 12 mm plywood and 25 mm lead line urethane foam placed internally and the driver back plastic caps pressed into foam. Based on the experimental results of the previous testing, however, it can be seen that the ringing was mildly higher than the best data achieved with array #2; In other words, pressing against the plastic caps was not as effective as applying clay to the caps.

Two CTS drivers numbered #45 and #53 were selected for the testing of a new urethane treatment. Both drivers have a G peak resonant frequency near the middle of the statistical range.

The new treatment consists of applying urethane (Devcon brand type Flexane 80) mixed with sand to the back plastic cap. First, CTS driver #45 was tested by applying a 5.6 mm thickness of the mixture to the back plastic cap and none on the plastic flange area. Anechoic chamber tone burst test results show that the level of driver ringing after a time span of 8.5 ms was reduced by about −11 dB (raw data not shown). This treatment was not as effective as we had hoped.

Secondly, a large amount of the urethane and sand mixture was molded around the entire the back cap region of driver #53. About 9 mm thickness was applied to the cap proper and the plastic flange area was covered with a thickness not less than 6 mm.

To test driver #53, the 76 mm aluminum sphere was suspended above the driver by about 1.8 m. Thus the round trip time of flight is about 10.7 ms. The transmitted burst was square, 6 cycles, 3600 Hz, 7 V-pk and driver had a 15 mH tuning inductor. Figure 43 shows the output signal for driver #53 with no damping of any kind. Note that at 8.5 ms the amplitude was 5.0 V-pp.

Figure 44 shows the output signal for driver #53 with the large amount of molded urethane and sand. Note that at 8.5 ms the amplitude is 0.38 V-pp. The reduction in ringing at this point is about −22.3 dB. This result is much better, though slightly worse than the best result with a clay treatment.
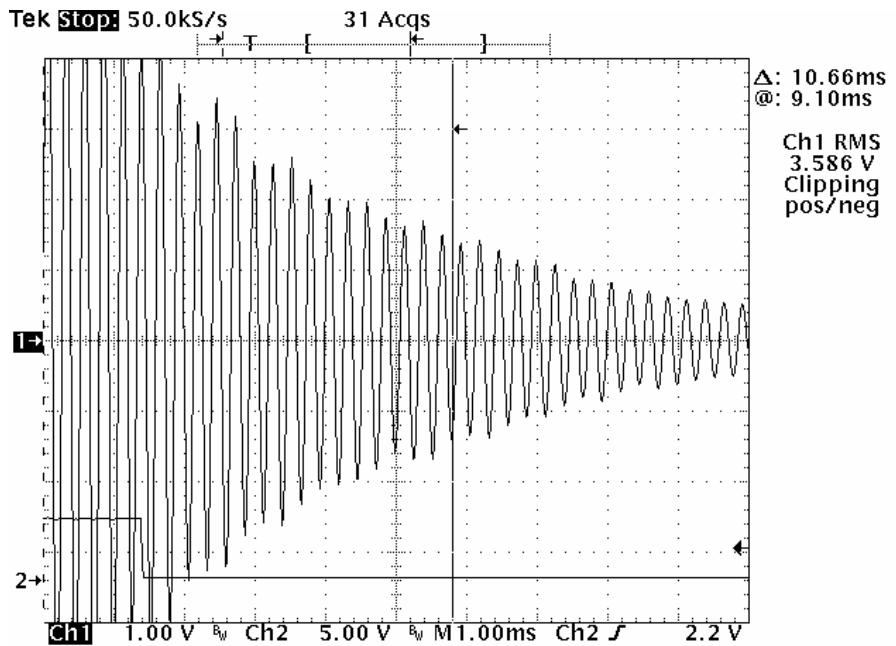
Figure 43.    Driver #53 with no damping of any kind. At 8.5 ms the amplitude is 5.0 V-pp.
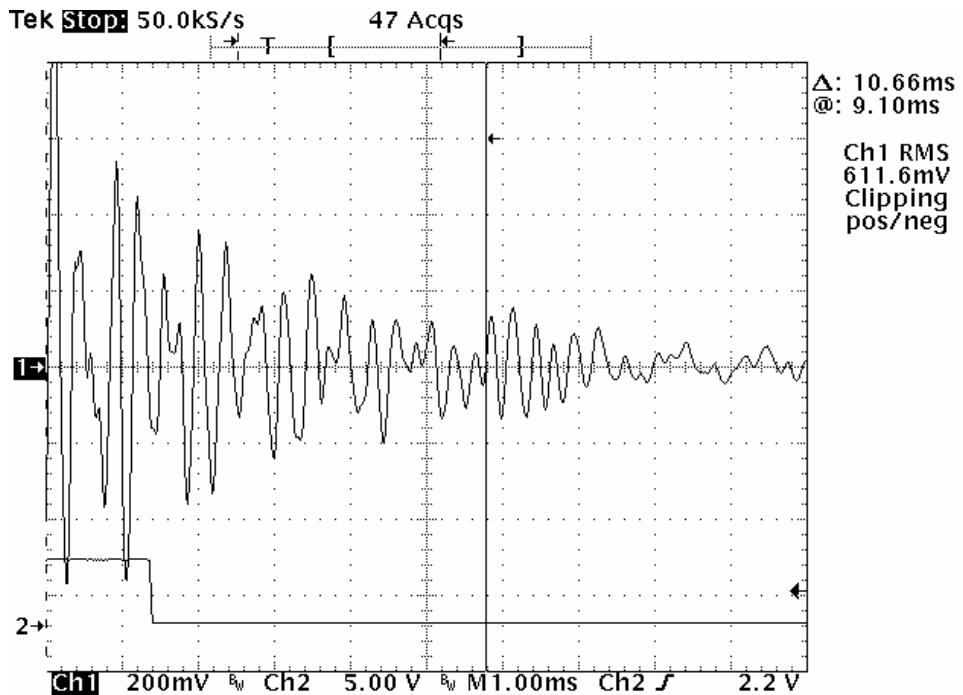


Figure 44.    Driver #53 with 200 mV vertical sensitivity. At 8.5 ms the amplitude was 0.38 V-pp. (1/13 reduction.)

THIS PAGE INTENTIONALLY LEFT BLANK

# IV.  CONCLUSIONS

This thesis investigated the potential sources of the long recovery time and distance for the transducer driver and array used at the Starfire Optical Range since 2001 for acoustic sounder measurements.  Several resonant sources were found and effective solutions were implemented to reduce the recovery time.  We also improved the receiving sensitivity of the echosounder and lowered the electronic noise of the preamplifier transducer combination.  We applied these techniques to a new array to verify that the long recovery time could be reduced.  A field test verified that a modified array had a recovery distance of 5 meters compared to 15 meters seen previously.

The primary problem in the piezo array was an acoustic standing wave at 4620 Hz that occurred between the back mounting plate and the bell of the transducer horn. Filling in the gaps between the horns with clay or eliminating the gaps by flush mounting the drivers were both effective solutions for this problem.   Small gaps or vertical edges in the flush mounting of the transducers were found to be detrimental and introduced interference in the transmitted and received signals.

 An additional problem was the resonant vibration of the back of the plastic transducer housing at a frequency around 3500 Hz.  The most effective solution to suppress this resonance was to use clay around the back of each transducer to dampen the vibration.  This was not an ideal solution since the 60C melting temperature of the clay could be exceeded when the array was exposed to mid-day desert temperatures.  Two attempts to use urethane on the plastic caps provided 11 and 20 dB suppression of the resonance.  This was not as effective as the 30 dB damping provided by the modeling clay.  Thicker urethane coatings with higher damping will need to be tried to get the maximum effectiveness.

Finally, the sound wave is radiated by the vibration of a paper cone attached to the bilaminar PZT disk. The paper cone has the advantage of low mass and good rigidity because of its shape, so its radiation efficiency is high. However, if the paper cone should

become wet, it would not function properly. Therefore, to avoid failure on a rainy day, the next major improvement should be focused on making the acoustic echosounder work well under all-weather conditions.

# LIST OF REFERENCES

1.    Frederick G. Smith, Atmospheric Propagation of Radiation, Vol. 2, Chap. 2, Bellingham, Washington: SPIE Optical Engineering Press, 1996.

2.    Moxcey, L.R., Utilization of Dense Packed Planar Acoustic Echosounders to Identify Turbulence Structure in the Lowest Levels of the Atmosphere, Master's Thesis, Naval Postgraduate School, Monterey, California, December 1987.

3.    David R. Cherry, Calibration of a High Frequency Monostatic Acoustic Echosounder, Master's Thesis, Naval Postgraduate School, Monterey, California, June 1993.

4.    Tatarski, V.I., Wave propagation in a Turbulent Medium, McGraw-Hill Book Company, Inc., New York, 1961.

5.    R.S. Lawrence, G.R. Ocus, and S.F. Clifford," Measurements of Atmospheric Turbulence Relevant to Optical Propagation," Journal of Optical Society of America, Vol. 60, No. 6, pp. 826-830, June 1970.

6.    Walters, D.L.,"Atmospheric Modulation Transfer Function for Desert and Mountain Locations: the Atmospheric Effects on $r_0$," Journal of Optical Society of America, Vol. 71, No. 4, pp. 397-405, April 1981.

7.    Walters, D.L.,"Atmospheric Modulation Transfer Function for Desert and Mountain Locations: $r_0$ Measurements," Journal of Optical Society of America, Vol. 71, No. 4, pp. 406-409, April 1981.

8.    Neff, W.D., "Quantitative Evaluation of Acoustic Echoes from the Planetary Boundary Layer," NOAA Technical Report ERL 322-WPL 38, June 1975.

9.    Harris, C.M.," Absorption of Sound in Air versus Humidity and Temperature," Journal of the Acoustical Society of America, Vol. 40, No. 4, pp. 148-159, 1966.

10.    Weingartner, F.J., Development of an Acoustic Echosounder for Detection of Lower Level Atmospheric Turbulence, Master's Thesis, Naval Postgraduate School, Monterey, California, June 1987.

11.    Wroblewski, M.R., Development of a Data Analysis System for the Detection of Lower Level Atmospheric Turbulence, Master's Thesis, Naval Postgraduate School, Monterey, California, June 1987.

12.    Oscar Bryan Wilson, An Introduction to Theory and Design of Sonar Transducers, Naval Postgraduate School, Monterey, California, June 1985.

13.     D. Stansfield, Underwater Electroacoustic Transducer, Bath University Press and Institute of Acoustics, UK, 1990.

14.     "Micro-Cap 7" student edition, Spectrum Software, Sunnyvale, California.

15.     S.N. Sen, Acoustics, waves and oscillations, Wiley Eastern Limited., New Delhi, India, 1990.

16.     Lawrence Kinsler E., Frey Austin R., Coppens Alan B., Sanders James V., Fundamentals of Acoustics, Fourth Edition, John Wiley & Sons, New York, 2000.

17.     Donald E. Hall, Basic Acoustics, Harper & Row, Publishers, Inc., New York, 1987.

18.     Harry F. Olson, Elements of Acoustical Engineering, D. Van Nostrand Company, New York, January 1942.

# INITIAL DISTRIBUTION LIST

1.      Defense Technical Information Center
       Ft. Belvoir, Virginia

2.      Dudley Knox Library
       Naval Postgraduate School
       Monterey, California

3.      Professor Donald L. Walters, Code PH/We
       Department of Physics
       Monterey, California

4.      Professor Thomas J. Hofler, Code PH/Hf
       Department of Physics
       Monterey, California